Document title:	GEM-TPC pre-design technical report
Description:	This document contains the pre-design of the GEM-TPC detector, as tracking detector for the Super-FRS at FAIR
Authors:	F. Garcia[1], C. Caesar[2], T. Grahn[3], A. Prochazka[2], B. Voss[2]
Organization:	[1]Helsinki Institute of Physics, University of Helsinki, 00014 Helsinki, Finland, [2]GSI Helmholtzzentrum für Schwerionenforschung, Darmstadt 64291, Germany [3]University of Jyväskylä, Department of Physics, 40014 Jyväskylä, Finland,

Abstract

This document contains the pre-design of the beam diagnostics components Tracking Detectors for the Super-FRS. A GEM-TPC detector has been suggested as suitable tracking detector for the ion/fragment beams produced at the in-flight separator Super-FRS under construction at the FAIR facility. The detector concept combines two widely used approaches in gas filled detectors, the Time Projection Chamber (TPC) and the Gas Electron Multiplication (GEM). Three detector generations (prototypes) have been tested in 2011, 2012 and 2014 with relativistic ion beams at GSI. Due to the high-resolution achromatic mode of the Super-FRS, highly homogeneous transmission tracking detectors are crucial to tag the momentum of the ion/fragment beam. They must be able to provide precise information on the (horizontal and vertical) deviation from nominal beam optics, while operated with slow-extracted beam on event-by event basis, in order to provide unambiguous identification of the fragments. The main requirements are a maximum active area horizontally and vertically of (380x80) mm^2, a position resolution of $\sigma < 1$ mm, a maximum rate capability of 1 MHz, a dynamic range of about 600 fC. About 32 tracking detectors operating in vacuum are needed along the Super-FRS beam line.

Table of contents

Content

List of Tables:

List of Figures:

1. Abbreviations, terms and definitions

Table 1.1: Abbreviations

Abb., Term	Definition
GSI	GSI Helmholtzzentrum für Schwerionenforschung GmbH, Darmstadt, Germany, in the following the Company
FAIR	International Facility for Antiproton and Ion Research
Super-FRS	Superconducting Fragment Separator
NUSTAR	NUclear STructure, Astrophysics and Reactions
TPC	Time Projection Chamber
GEM	Gas Electron Multiplication
PS	Pre-Separator
MS	Main-Separator
HEB	High Energy Branch
LEB	Low Energy Branch
RB	Ring Branch
FRS	Fragment Separator
FEE	Front-End Electronics
DAQ	Data Acquisition
RIBs	Rare Isotope Beams

2. FAIR Super-FRS tracking detector concept

A GEM-TPC detector, which combines two different gas-filled detectors, the Time Projection Chamber (TPC) and the Gas Electron Multiplication (GEM), has been suggested as tracking detector for the ion/fragment beams produced at the in-flight separator Super-FRS under construction at the FAIR facility. The main properties of the Super-FRS are given in Appendix I and the physics case in Appendix II.

2.1. System overview

The tracking detectors of the Super-FRS are expected to measure the space coordinates of the slow-extracted ion/fragment beam, i.e. transversal (horizontal and vertical) to the beam axis, event by event. Operating in pair at the same station (or focal plane) they provide the horizontal and

vertical angles of the ion trajectory. The location of the tracking detectors along the Super-FRS is shown in Figure 2.1. Three areas are considered: the Pre-Separator (PS), the Main-Separator (MS) and the Energy Buncher (EB) (see Appendix I). The total number of detectors per station is listed in Table 2.1.

Station	Unit	Separator region
FPF2	4	PS
FPF3	1	PS
FPF4	2	PS
FMF1	2	MS
FMF2	4	MS
FMF2a	4	MS
FMF3	2	MS
FHF1	2	MS
FHF1a	2	MS
FLF1	1	MS
FLF2	2	MS
FRF3	2	MS
FLF4	1	EB
FLF5	2	EB
FLF6	1	EB

Table 2.1: Tracking detectors at the Super-FRS stations. PS=Pre-Separator, MS=Main-Separator and EB= Energy Buncher of the Super-FRS.

They are operated in vacuum inside the beam diagnostic chamber, except at FMF2a, FHF1a and FLF6, where some units are foreseen to be mounted and working in air, depending on the particular experiment. Each detector inside the vacuum chamber is vertically movable along the transversal beam cross section. The movement is conducted by stepper motor driven linear actuator on an installation flange. All detectors have to be handled from the top. While inserted they will provide the horizontal and vertical ion position measurement event by event. The design of the tracking detectors installed in the PS region, i.e. at FPF2, FPF3 and FPF4, must support robot handling. In Fig. 2.2, the schematic construction of a gas filled tracking detector is shown. It combines the Time Projection Chamber (TPC) and the Gas Electron Multiplication (GEM). The tracking detectors are mounted in a ladder. The same ladder is used to accommodate the beam profile detectors.

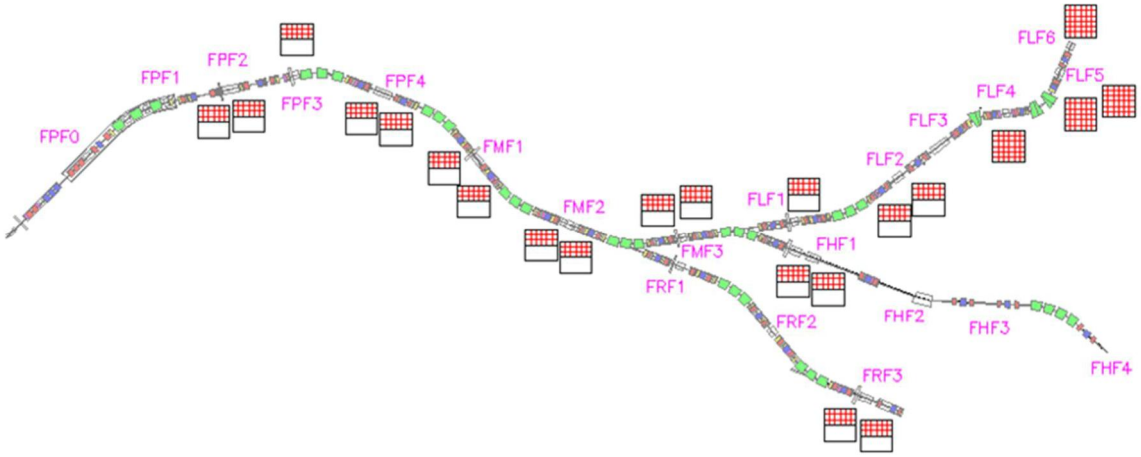

Figure 2.1: Layout of the Super-FRS and tracking detectors (red symbols). At all focal planes, except FLF4, FLF5 and FLF6, each tracking detector is integrated in a ladder.

2.2. Parameter requirements

The tracking detectors of the Super-FRS must be able to provide information on the deviation from nominal beam optics, while operated with slow-extracted beam on event-by event basis. Moreover, in the MS they are used to tag the momentum of the ion/fragment beam, in order to provide unambiguous fragment identification in mass.

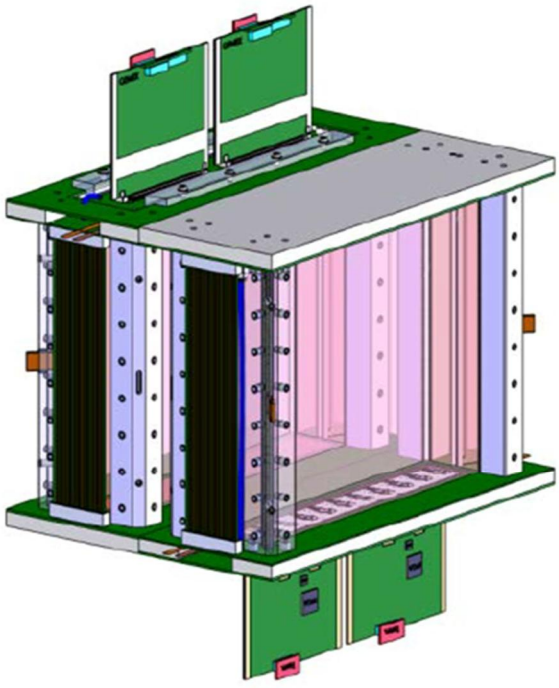

Figure 2.2: Schematic construction of the GEM-TPC detector.

Due to the high-resolution achromatic mode of the Super-FRS, the tracking detectors are crucial to obtain a precise momentum measurement of the produced fragments. They can be also used to apply a position correction of the ion velocity, whenever needed.

The technical design is defined by the main beam parameter (e.g. beam energy and intensity, electric charge, duty cycle, etc.). At the Super-FRS high-energy primary and secondary fully stripped ion beams can be used up to uranium (see Appendix I).

The Super-FRS tracking detectors should operate up to few MHz beam intensity close to 100% efficiency at the stations FPF4, FMF1, FMF2, FMF3, FHF1, FLF2 and FLF4. At the focal planes FPF2, FPF3, FLF1, FRF3, FLF5 and FLF6 having high detector efficiency is not mandatory.

The technical specifications of the tracking detectors are listed in Tables 2.2 and 2.3.

Device	Parameter	Value	Unit
Tracking detector operated in vacuum			
	largest beam spot size	380x150	mm^2
	Maximum allowed length (in beam direction)	See Table 2.3	
	Horizontal position resolution	+/- 0.2	mm
	Vertical position resolution	+/- 0.2	mm
	Positioning	+/- 0.1 mm	mm
	time resolution	<3	ns
	Maximum rate capability	1	kHz/mm^2
	Dynamic range	600 (see Section 11)	fC
	Gas	P10 or other	
	Minimum active area	see Table 2.3	
	dE/E	see Section 11	
Tracking detector operated in air			
	largest beam spot size	380x80	mm^2
	Horizontal position resolution	+/- 0.2	mm
	Vertical position resolution	+/- 0.2	mm
	time resolution (FWHM)	<3	ns
	Maximum rate capability	1	kHz/mm^2
	Dynamic range	600 (see Section 11)	fC
	Gas	P10 or other	
	Minimum active area	see Table 2.3	
	dE/E	see Section 11	

Table 2.2: Technical specification of the tracking detectors.

Focal plane	X(mm)	Y(mm)	Z(mm)	Separator region
FPF2	380	80	250	PS
FPF3	380	150	250	PS
FPF4	200	80	400	PS
FMF1	380	80	400	MS
FMF2	380	80	400	MS
FMF2a	380	80	400	MS
FMF3	380	80	400	MS
FHF1	200	80	400	MS
FHF1a	200	80	400	MS
FLF1	380	80	250	MS
FLF2	200	80	400	MS
FRF3	200	80	250	MS
FLF4	380	150	400	EB
FLF5	380	150	250	EB
FLF6	200	80	250	EB

Table 2.3: Minimum active area and maximum allowed length in beam direction of the tracking detectors.

2.3. The GEM-TPC detector

The TPC part of the detectors is based on the design of the time-projection chamber detectors used at FRS at GSI for beam tracking. The present design is a novel concept that combines the TPC detector with the GEM detector as an amplification stage [1]. It also will reduce the ion feedback impairing the resolution and efficiency of the standard TPC detectors. The GEM-TPC [2] to be developed must have high electron-field homogeneity along the charge-carrier drift field of the TPC chamber, low GEM-foil leakage current, high amplification of each of the GEM-foil levels and fast signal readout. In addition, the signal to noise ratio needs to be high.

Due to high radiation-level environment, detectors that will be installed for the beam diagnostics are expected to be operational as long as possible without any need for human intervention. Therefore, the production quality control is of great importance.

The optimization of the GEM-amplification stage is important for operating at high rates. To avoid decline in efficiency and in resolution, the field uniformity inside the TPC drift volume has to be optimized.

The GEM-TPC detectors for particle tracking in the main separator will be operated in twin field cage configuration with two twin detectors at almost each focal plane. Such a configuration will unambiguously detect the particle track (x, y, z coordinates at the entrance and exit) and thus magnetic rigidity ($B\rho$) can be deduced. The idea behind the twin field cage configuration is to achieve 100% tracking efficiency even at highest rates (10 MHz). The concept of the twin GEM-TPC detector working in air is shown in Figure 2.3 and will be described in the following sections.

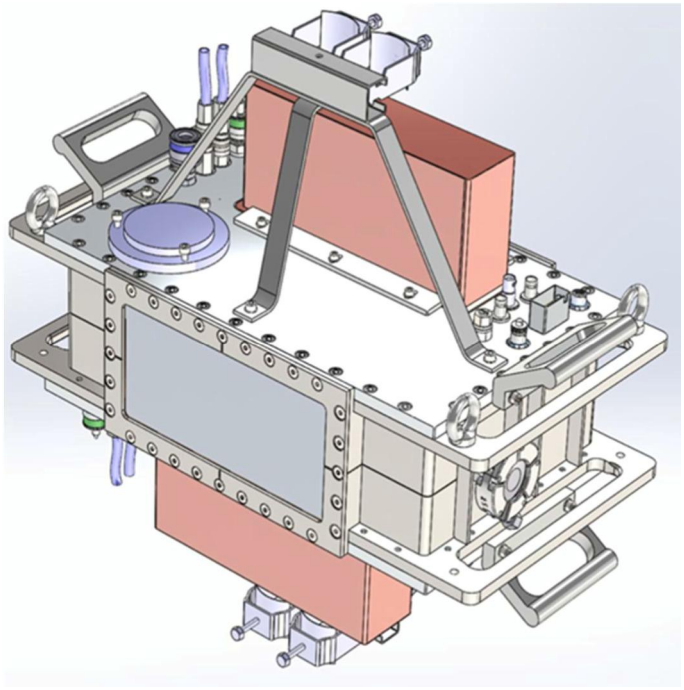

Figure 2.3: The twin GEM-TPC detector.

3. Mechanical structure and its components

3.1. Introduction

The version of the GEM-TPC detector described herein is based on a twin configuration of two identical active volumes, each enclosing a drift a volume of rectangular or ‘boxed’ shape with a constant electrical field with up to 320 V/cm of strength. The direction of the fields has been chosen to be in vertical axis (‘Y’) perpendicular to the beam of traversing particles, their orientation is opposite within the two volumes following each other along the beams path (‘Z’). The centers of the two field cage compartments are adjusted to be on one line in all directions. A sketch of this arrangement is shown in Figs. 3.1 and 3.2.

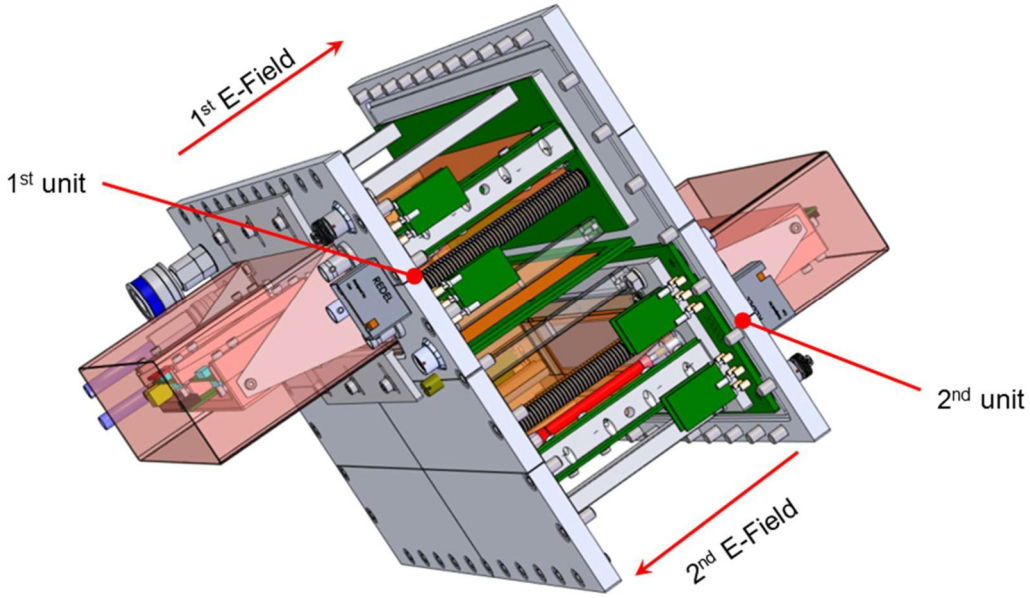

Figure 3.1: CAD sketch of the field-cage compartments of the Super-FRS TwinGEM-TPC.

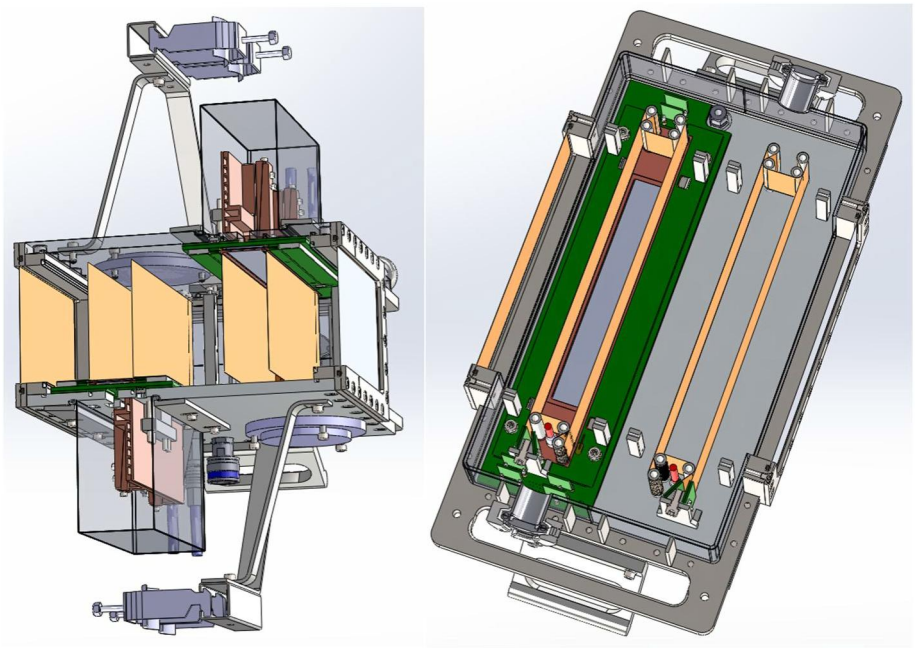

Figure 3.2: CAD sketch of the field-cage compartments of the Super-FRS TwinGEM-TPC demonstrating their arrangement and the various thin layers of material the beam has to pass (horizontally from left to right).

3.2. Housing and Vessel

The housing of the detector has been realized in two types of constructions:

a) made from stainless steel in a welding-type design as shown in Fig. 3.3 as well as
b) a full-block machined aluminum body shown in Fig. 3.4

The current design of the housing vessel allows a precision mounting of the two compartments of the TwinGEM-TPC relative to each other with an accuracy of better than 0.1 mm in all directions.

Both types allow operation under reduced pressure of e.g. 0.3 mbar up to an overpressure of approximately 1 bar. The welded-type specimen of the vessel can be either pumped down to several mbar and/or may be applied in a vacuum surrounding by the appropriate choice of foils of the entrance and exit windows made of either 25 μm thick Kapton or stainless steel of 50 μm thickness.

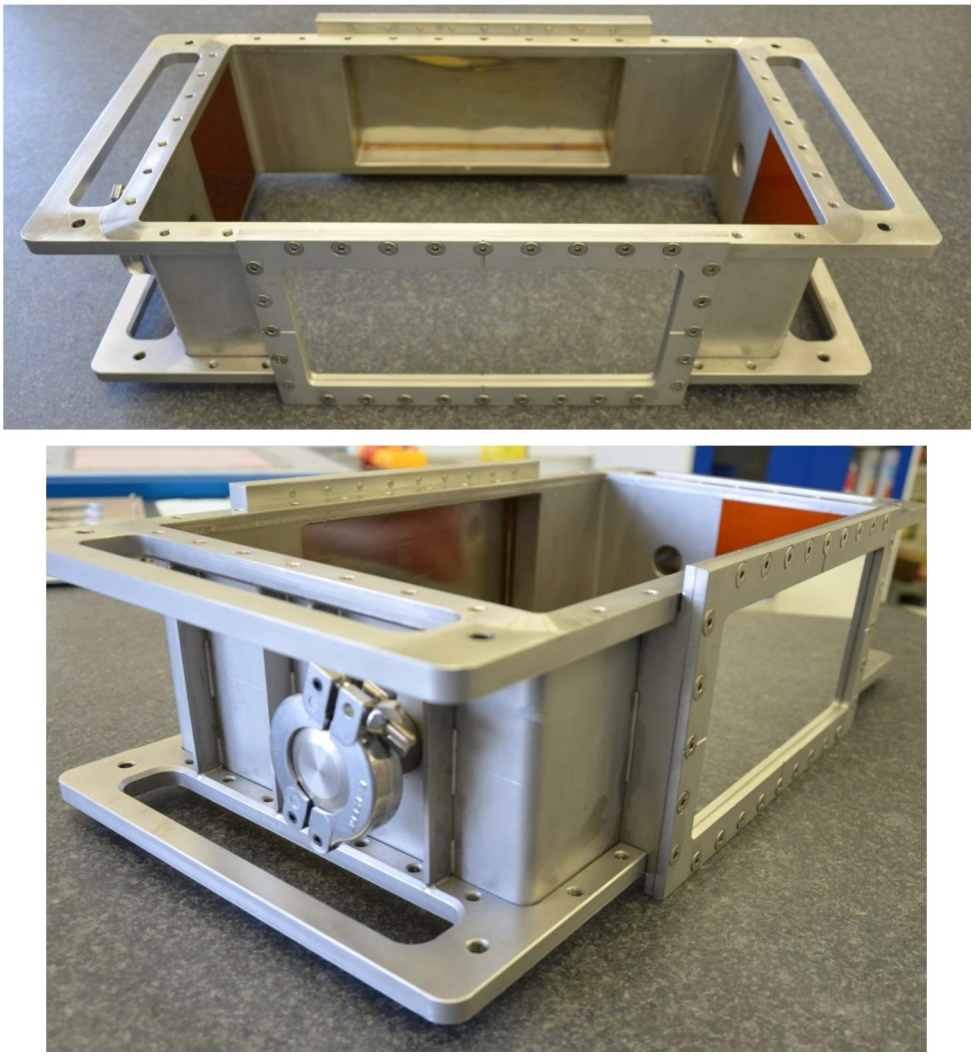

Figure 3.3: Housing made from stainless steel in a welding-type construction. The KF-type exhausts can be used to evacuate the vessel enforcing out-gassing of the detector materials installed inside in order to achieve better gas-purity.

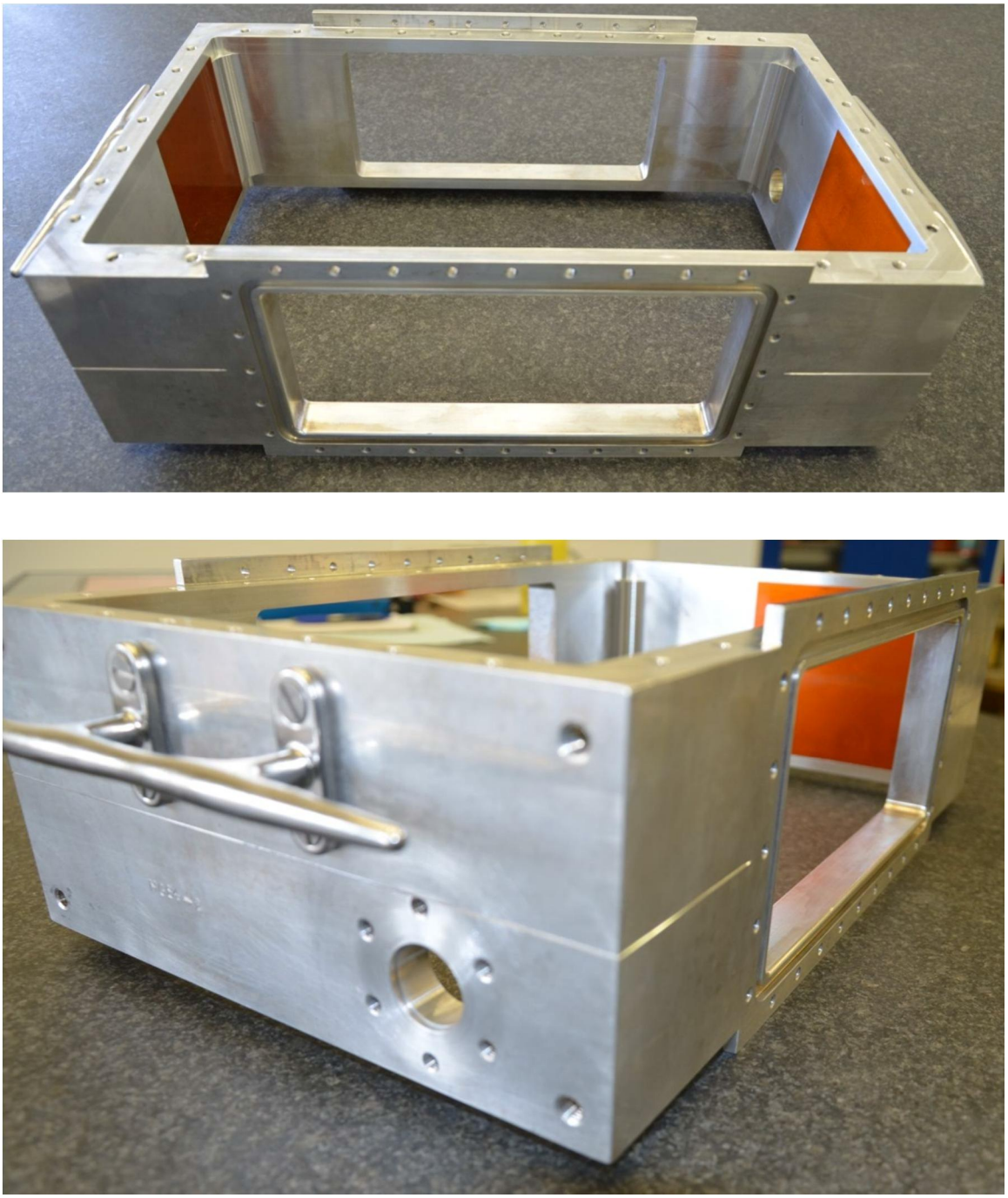

Figure 3.4: Housing milled-out from a single block of Aluminum.

3.3. Flanges

Due to these principal design rules, the whole setup of the two opposing compartments of the 'Twin' configuration of the GEM-TPC were set up essentially identical.

On overview picture of a single panel of the ‘Twin’-type GEM-TPC is shown in Fig. 3.5. The two groups of supplies (electrical and fluidal) as well as high-density connectors for the read out of the signals are clearly discriminable. Line-engravings are realized for LASER adjustment together with a bubble-level.

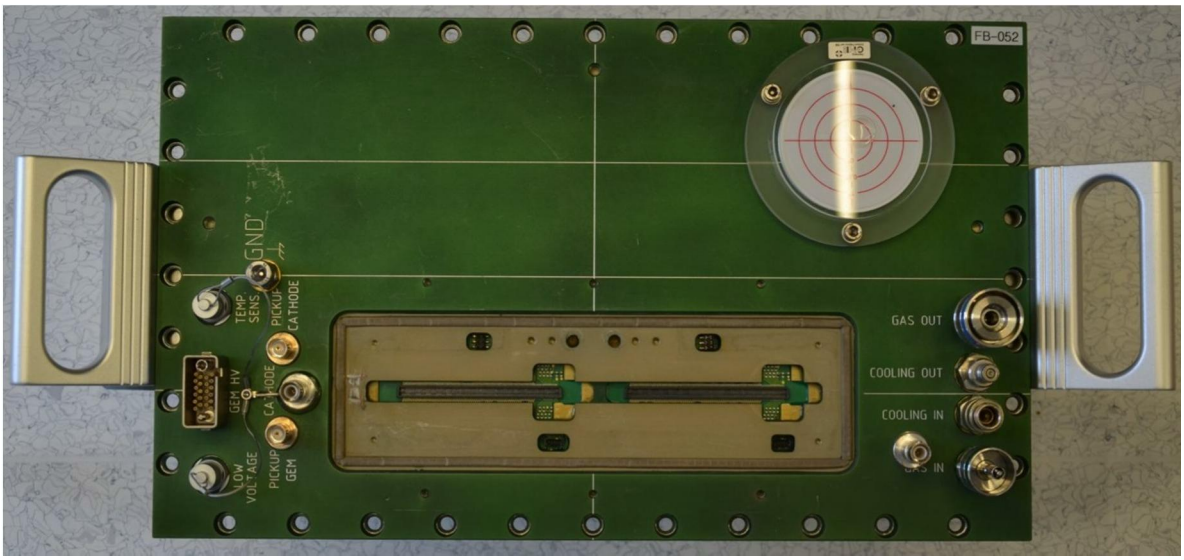

Figure 3.5: Overview picture of one of the flanges mounted to the ‘Twin’-type GEM-TPC facing the surrounding abient.

In order to maximize compactness, the actual flanges also serve to distribute all electrical and fluidal supplies as indicated in Fig.3.6. Moreover, they provide appropriate stiffening of the pad-planes glued to them in order to achieve optimal flatness of the pad plane PCB. They are part of the screening concept against electromagnetic interferences and close the Faraday cage together with the metallic vessel of the detector.

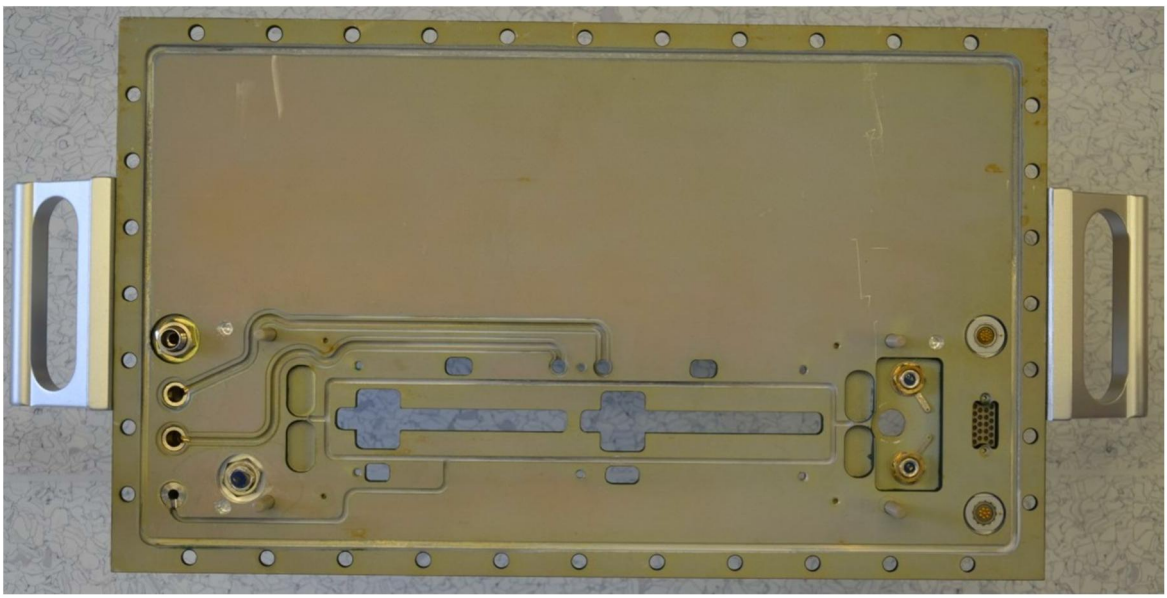

Figure 3.6: Overview picture of one of the back-side of the flanges mounted to the 'Twin'-type GEM-TPC facing the inside volume of the detector. The two groups of grooves as part of the distribution of the fluidal-supplies are visible as well as the screw-mounted connectors.

3.4. Adjustment

Ease of operation was another principal design goal to be achieved for the detector. Thus, several design details have been realized as shown in fig. 7 in order to facilitate adjustment.

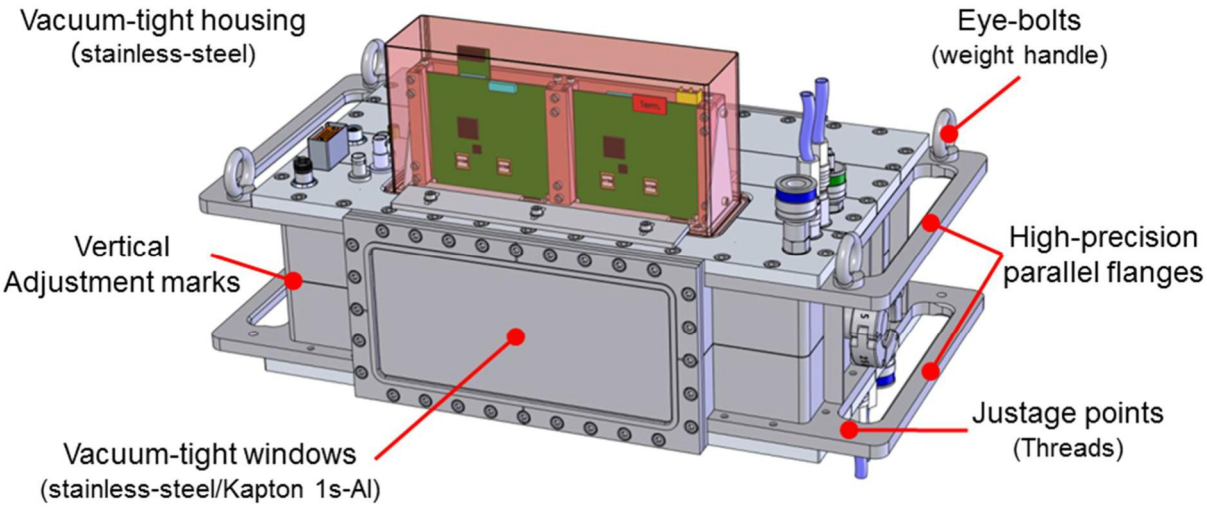

Figure 3.7: CADS sketch of the chamber housing emphasizing various design details which support the adjustment during mounting.

Moreover, a bubble-level device (see Fig.3.8) with an accuracy of 0.1° is installed on the top-level flange (see Fig. 3.5) which helps to ease adjusted mounting of the chamber at least horizontally

which is especially helpful in a crowded experimental surrounding where the Laser might not reach the chamber surfaces.

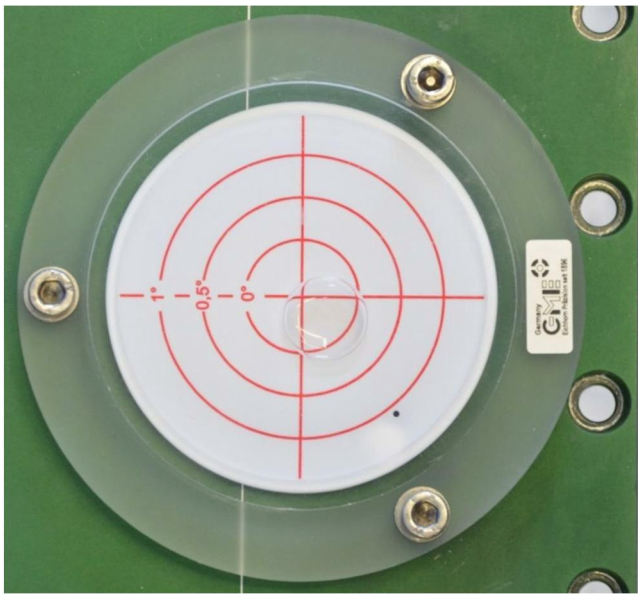

Figure 3.8: Picture of the bubble-level device mounted on the top panel of the TwinGEM-TPC allowing a horizontal adjustment of the detector.

In addition, centered marks on the vessels (see Figs. 3.3 and 3.4) as well as corresponding engravings on the panel-flanges (see Figs. 3.5) allow for an adjustment with the help of external Laser lines with an accuracy of down to 0.1 mm, depending on the achievable width of the LASER lines.

3.5. Supplies and Connectors

Two groups of supplies were grouped together to facilitate interconnection during mounting of the detector system.

a) The electrical supplies and slow-control signals like ground (GND), low- and high- bias voltages; sensor- and pickup-signals (see Fig. 3.9).
b) The fluidal supplies as the detector gas as well as the cooling fluid (see Fig. 3.10)

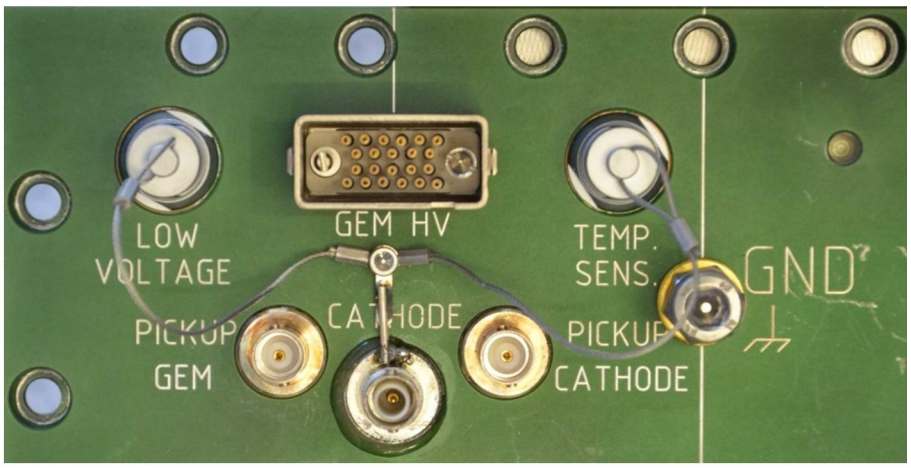

Figure 3.9: Picture of the electrical supplies and signals: Ground (GND), low- and high- bias voltages, sensor- and pickup-signals.

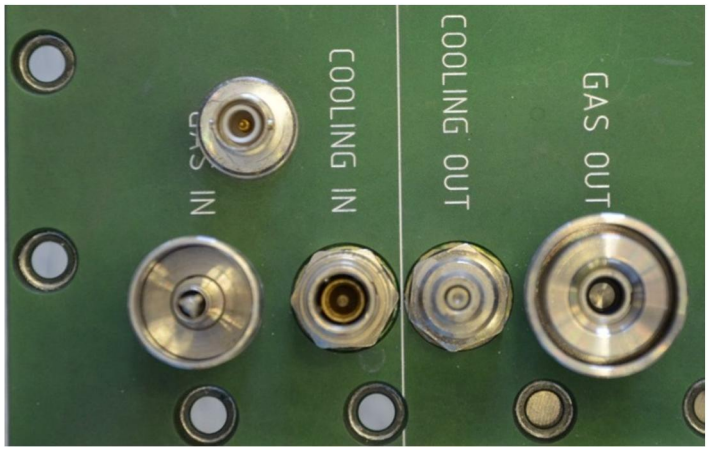

Figure 3.10: Picture of the fluidal supplies, the detector gas as well as the cooling fluid. Note that it has been decided only after the flanges have already been produced to provide the 1st strip of the field cage with an autonomous biasing.

In order to ease connection and to avoid errors, coded self-closing valves have been selected for all fluidal media.

3.6. Cooling system

The current version of the read-out ASIC (XYTER-type NX1.0 and NX1.1) as well as the following detector-near digital read-out chain (ADC & FPGA) require active cooling and a stabilized (± 1°C) temperature. In order to facilitate the supply with the appropriate water-based cooling fluids, the distribution of the coolant was designed into the Aluminum flange (see Fig. 3.6) offering in- and outlet via a connectors with self-closing valves.

A picture of the actual cooler is shown in Fig.3.11 without and in Fig. 3.12 with the cover heat-screen removed and the actual GEMEX1C read-out boards installed (the interlinking GEMCON2 PCB bridge has been removed too).

Figure 3.11: Picture of the active copper cooler.

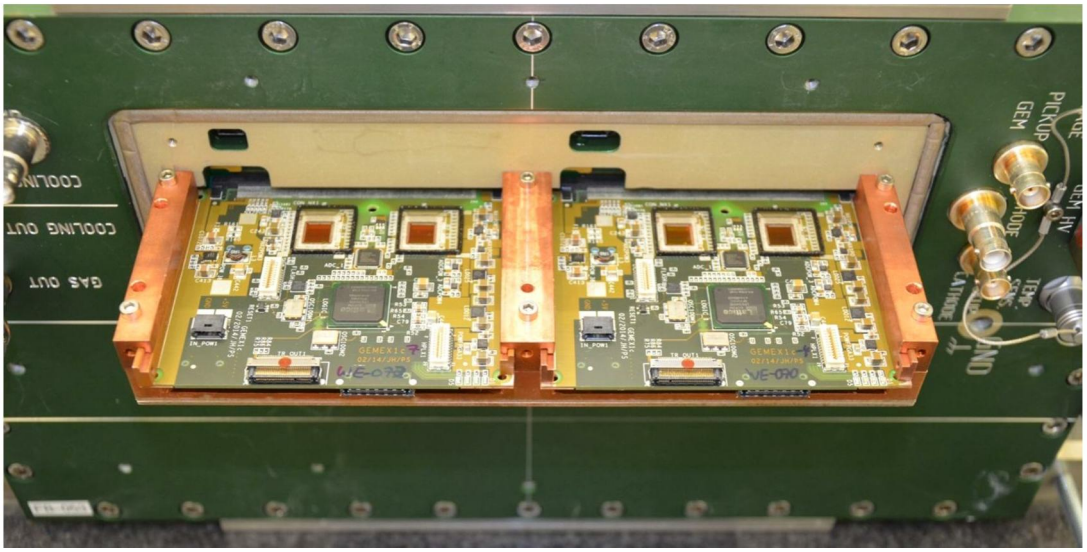

Figure 3.12: Picture of the active copper cooler with the cover heat-screen removed and the actual GEMEX1C read-out boards installed (the interlinking CEMCON PCB bridge has been removed too).

3.7. Gas system

The gas-distribution systems are integrated into the detector panel as well as into the cathode plate (see Figs. 3.10).

Each compartment of the GEM-TPC in ‘Twin’ configuration is provided with an autonomous supply.

Inside the vessel, fresh gas is directly supplied into the respective induction gap (the volume just above the PadPlane, facing GEM-layer #3) of each field-cage compartment via the pad-plane. The corresponding exhausts are part of the cathode support structure of each compartment. This allows for a more or less guided flow across each drift volume.

3.8. Diagnostic station

An example of Super-FRS diagnostic station [4] (FPF2) is shown in Figure 3.13. The dimension of vacuum flanges in the beam direction is limited by the presence of the other beam diagnostics components. This is one of the main reason of having tracking detectors and profile monitors on the same ladder/drive. The maximum length of the vacuum flanges of the tracking detector at each station is shown in Table 3.1.

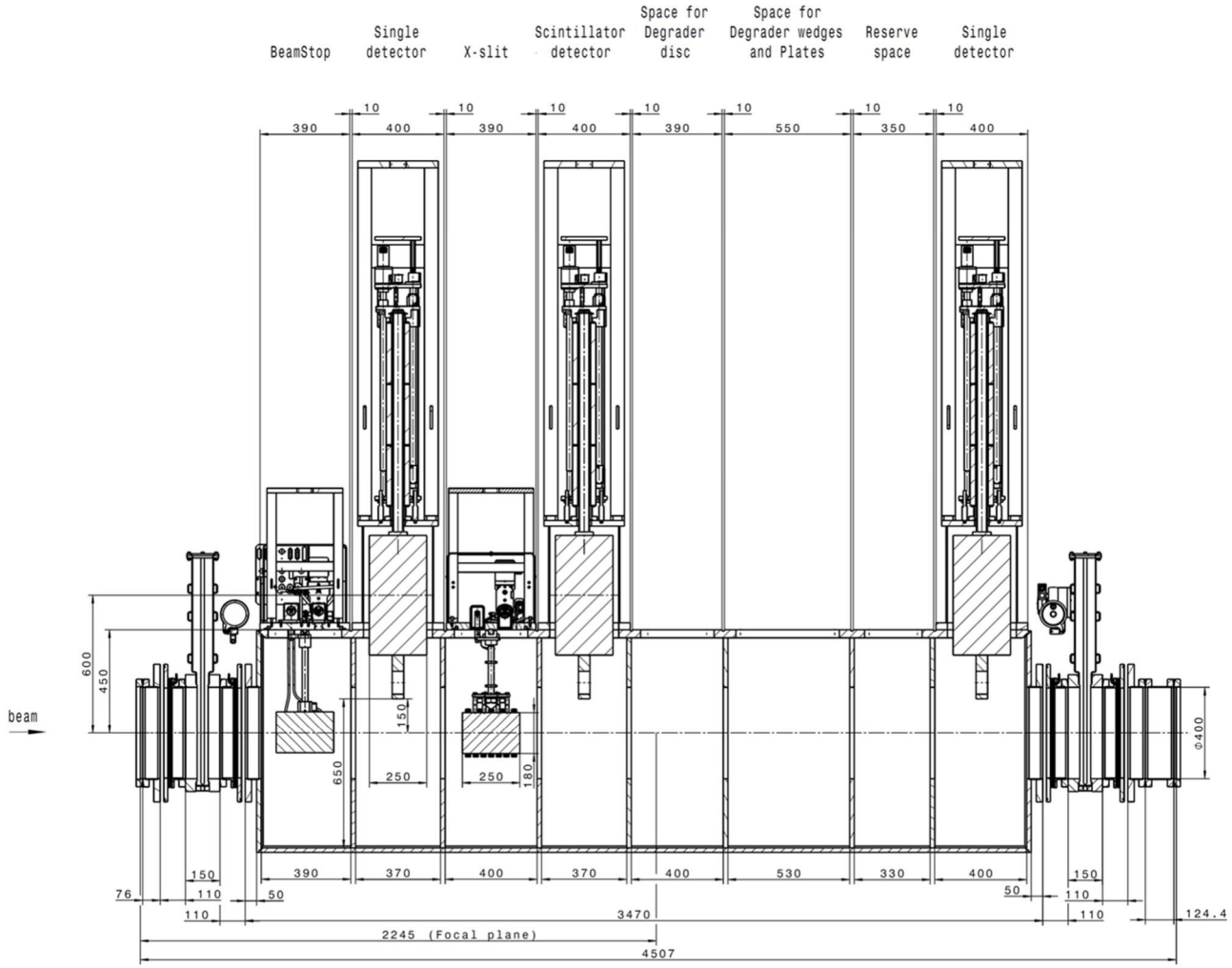

Figure 3.13: Super-FRS diagnostic chamber at FPF2.

Focal plane	Z(mm)	Separator region
FPF2	400	PS
FPF3	400	PS
FPF4	550	PS
FMF1	550	MS
FMF2	550	MS
FMF2a	-	MS
FMF3	550	MS
FHF1	550	MS
FHF1a	-	MS
FLF1	400	MS
FLF2	550	MS
FRF3	400	MS
FLF4	550	EB
FLF5	400	EB
FLF6	-	EB

Table 3.1: Maximum allowed flange dimension along the beam direction.

3.9. Actuator and ladder

The GEM-TPC detector is attached on the ladder arm that in turn is used to move the detector vertically using a standard linear actuator stepper motor. In addition the ladder arm is used to guide cables, gas and cooling pipes from the detector to outside the vacuum chamber. The connectors are situated on the top flange of the detector and at the other end on the top flange of the ladder arm. The SEM-Grid beam profile detector is situated on the same ladder arm beneath the GEM-TPC detector. In the pre-separator section the ladder arms are operated by a robot. The schematic design of the ladder is shown in Fig. 3.14.

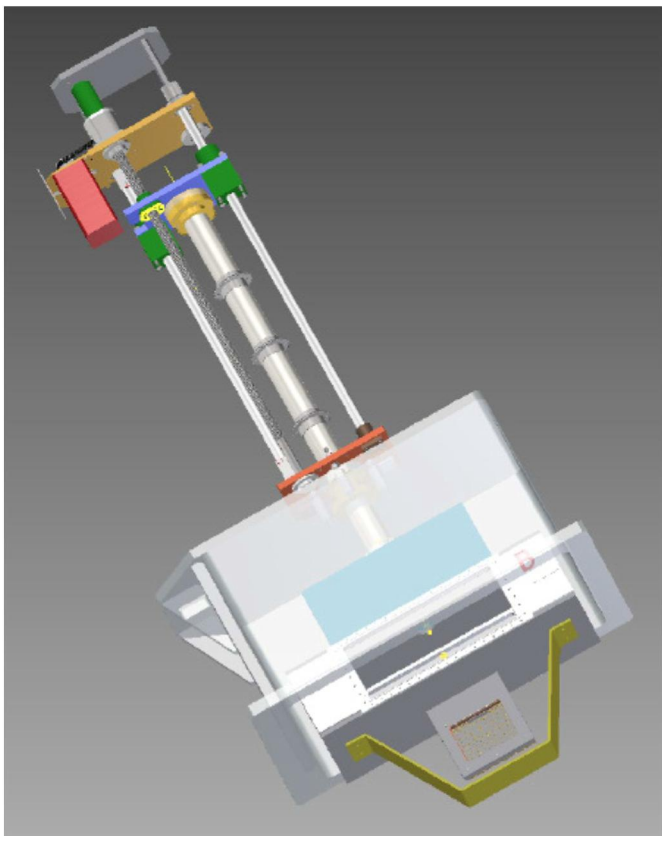

Figure 3.14: GEM-TPC detector attached on to the ladder arm. The SEM-Grid beam profile monitor is attached on the bottom flange of GEM-TPC.

4. Gas choice

The choice for the gas has been main driven by the parameters of the lateral diffusion, which is or de order of 1 mm for 10 cm long drift and due to the fact that previous TPC were operating on P10 gas and it was needed to have the possibility for a direct comparison.

5. HV power supply

The powering scheme for a GEM based TPC needs to be adequate to accommodate the two different circuits that intrinsically are on this type of detectors. On one hand, there is the high voltage needed for the field cage, however a relative low current is flowing though it on the other hand the GEM stack which will need moderate high voltage and high current, needed for handling the high rate. Therefore in order to manage such a system a set of two power suppliers is needed to operate the GEM-TPC and the scheme is shown in Fig. 5.1. It can be seen that the HV_1 is connected to the cathode of the TPC and the HV_2 is connected to the top of the first GEM. This will allow to full fill the requirements in terms of providing different currents values required by these components. One important aspect of this particular powering scheme is that one has to level out

the potential on the last strip and the one of the top of the first GEM in such a way that the potential is the same.

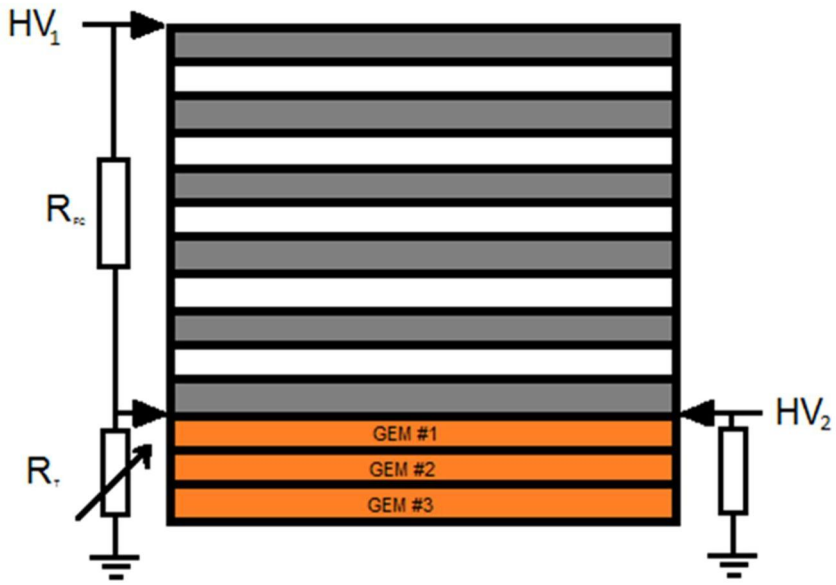

Figure 5.1: GEM-TPC high voltage power scheme.

5.1. Field cage power supply

The main purpose of the powering for the field cage is to be able to apply a field gradient across the volume of the field cage in such a way that the electrons drift towards the GEM amplification stage. Therefore in order to have the maximum uniformity the potential difference between strips need to be as small as possible. Results from simulations show that field becomes very uniform in the enclosed volume, after a distance two times the strips pitch from the wall, therefore charge produced by particles crossing the sensitive volume of the chamber close to the walls will end up in a metallic plate, located on the top of the first GEM. The field cage together with a set of dividers is shown in the Figure 5.2. It is important to highlight that the foil used for the field cage has double sided strips with is intended for a better field uniformity at the pitch of 3 mm on each side.

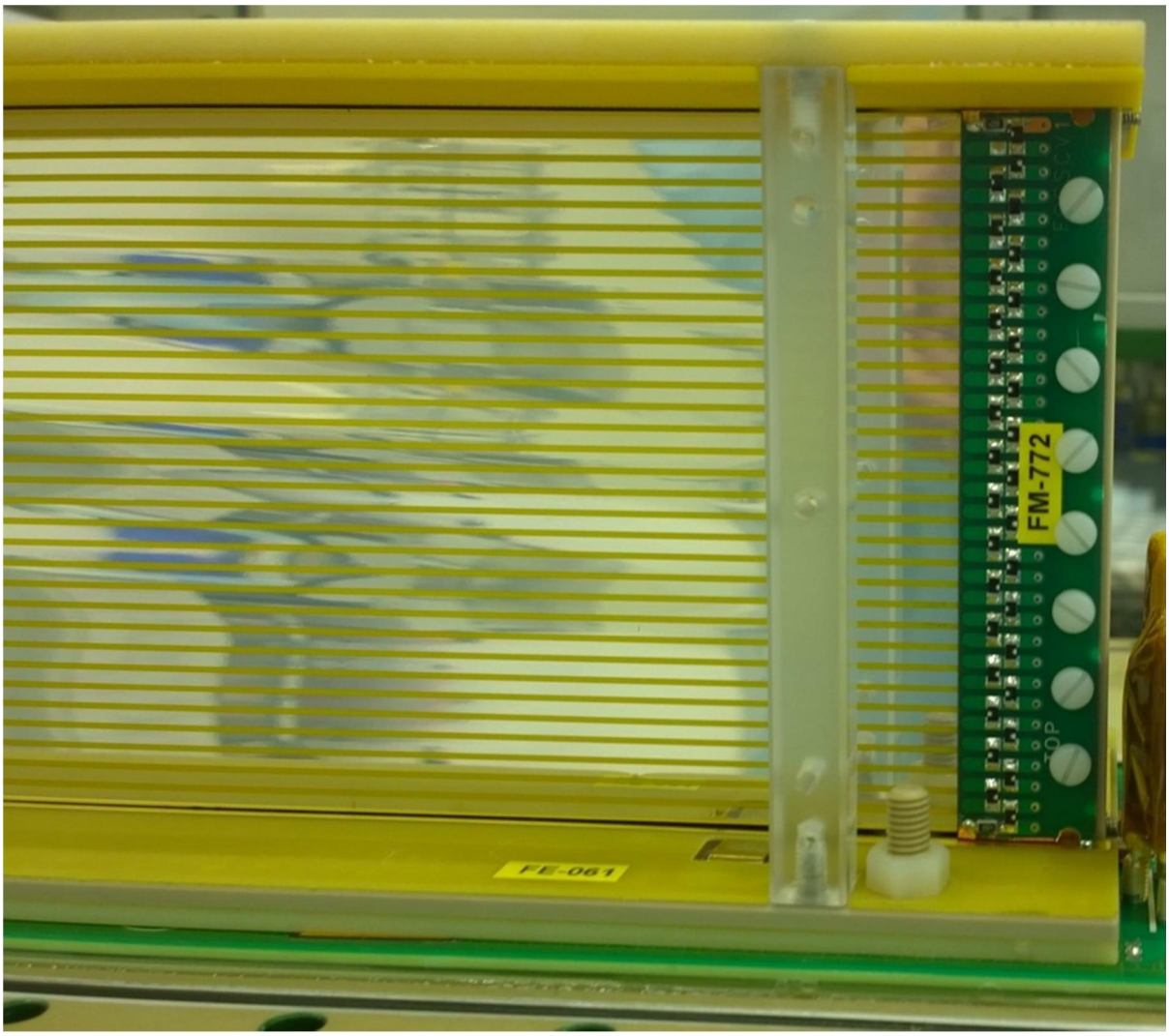

Figure 5.2: Field cage resistor divider.

The divider itself has a set of 33 resistors, with total resistance of 100 MΩ and the current circulating across the field cage was calculated to be in the order of tens of μA depending on the field to be applied inside the field cage. For example if one decided to use a field of 150 V/cm, thus having a total drop on the divider of 1.5 kV, then this will give a 15 μA current circulating through it. In order to have the possibility to set the potential at the last strip of the field cage a resistor terminator has been developed. The main purpose of this device was to be able to adjust the potential depending on what was the potential selected for the top of the first GEM. This was possible by the use of a high voltage potentiometer connected to ground. In the Fig. 5.3 the picture of the device is shown. Below it can be seen that the device has two channels one per field cage and in order to produce the total resistance required two potentiometers and one fixed resistor were cascaded. Thus allow us to scan fields between 150 V/cm up to 320 V/cm for a very low gain of the GEM stack. In order to clearer illustrate the function of this device see Fig. 5.1 marked with the name RT.

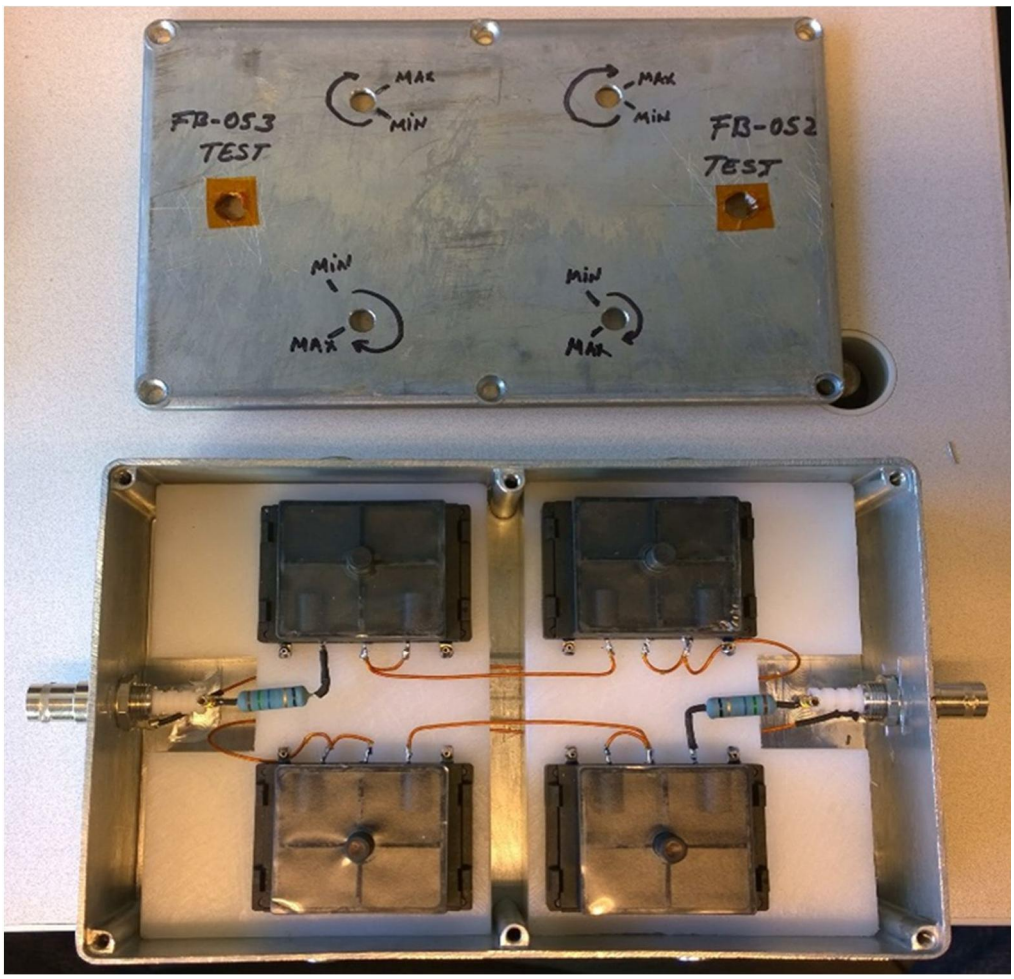

Figure 5.3: Field cage resistor terminator.

5.2. GEM Stack power supply

The GEM stack used for this chamber is a triple GEM. Therefore a set of 6 high voltage power lines is needed to be supplied, however the connection looks the same as a commonly used triple GEM detector, where the voltage potential for each GEM are provided via a passive resistor divider. The illustration of the powering scheme is shown in the Fig. 5.4.

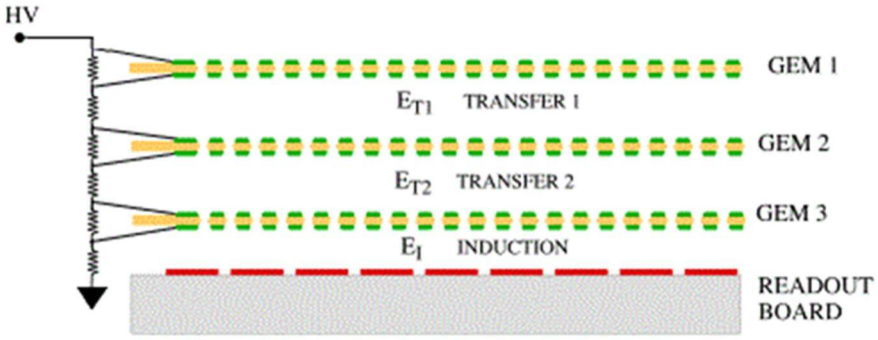

Figure 5.4: GEM stack power scheme.

The resistor divider used for the tests was the same as the one used for the TOTEM triple GEM [5] detector, with the main characteristics of this divider are two: the first one is that the field between the transfers and induction gaps is keep close to 3 kV/cm and the gain on the GEMs is higher at the bottom. It is important to highlight that we can achieve modulation of the gains from tens u to hundred thousands, which is needed at the super-FRS since the specimens to detect varies from very light ions, e.g. hydrogen, up to uranium. In this way we can managed to avoid saturation of the electronics.

The divider used for the prototypes is shown in Fig. 5.

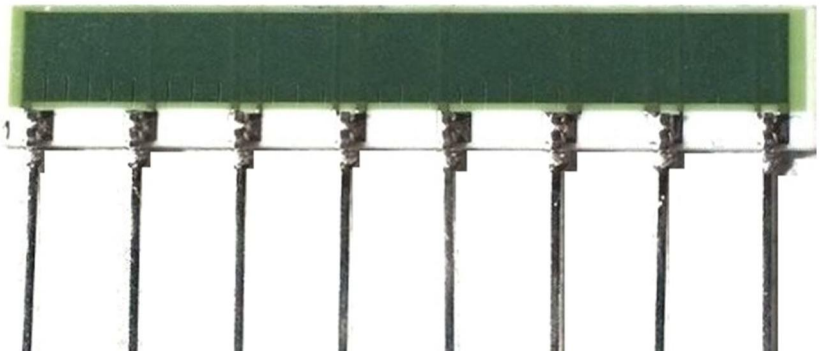

Figure 5.5: GEM stack passive divider.

6. Readout pad-planes

Each field-cage compartment of the 'Twin' configuration of the Super-FRS GEM-TPC is equipped with an identical pad-plane which can be operated 'stand-alone'. This optimizes mass-production and eases maintenance by minimizing the amount of different parts to be held on stock as well as by reducing the number of processes for their fabrication and assembly.

The PCB realizes all routes required for the high-voltage distribution for all electrical supplies such as GEM-layers, HV-filters, low-voltage for the read-out boards and various temperature sensors. Moreover it provides sockets for the high-voltage filters as well as pick-up capacities and the outlets of the gas-distribution system. It directly connects to all electrical connectors mounted on the respective panel, except the cathode high-voltage, replacing all cables inside the detector volume which would be required otherwise.

A picture of the actual pad-plane PCB mounted on one of the panel-flanges of the TwinGEM-TPC is shown in Fig. 6.1.

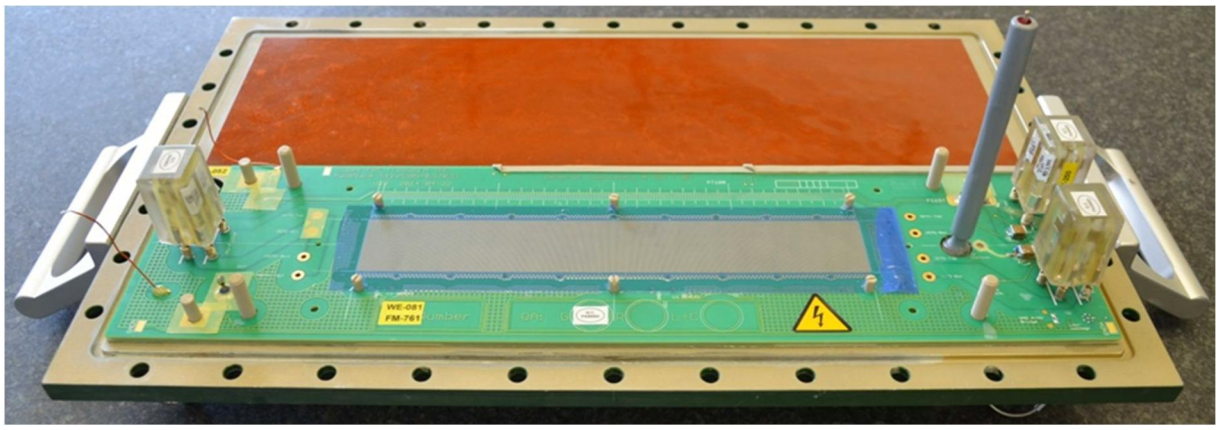

Figure 6.1: Picture of the actual pad-plane mounted on one of the panel flanges of the Super-FRS Twin_GEM-TPC.

The pad-plane PCB-sandwich itself consists of two separately produced parts which are merged/ glued together during assembly at GSI:

a) A backing provides insulation and screening as well as sealing of the various fluids fed to the detector via the panels. Through its thickness it also helps to minimize the capacity of the signal lines with respect to ground and it provides additional stability and flatness for the sandwich.

b) The actual 'signal' PCB is distributing low- and high-voltage of the supplies and realizes the routing of the electrical signals to be picked up inside the active volume and read out via the front-end boards of the read-out system which are flanged to the panels.

6.1. Geometry

Figure 6.2 shows a snap shot of the surface of the pad-plane of the Super-FRS GEM-TPC facing the gas volume. The inner 'active' area is patterned with 512 strip-type electrodes forming the projection layer of the detector.

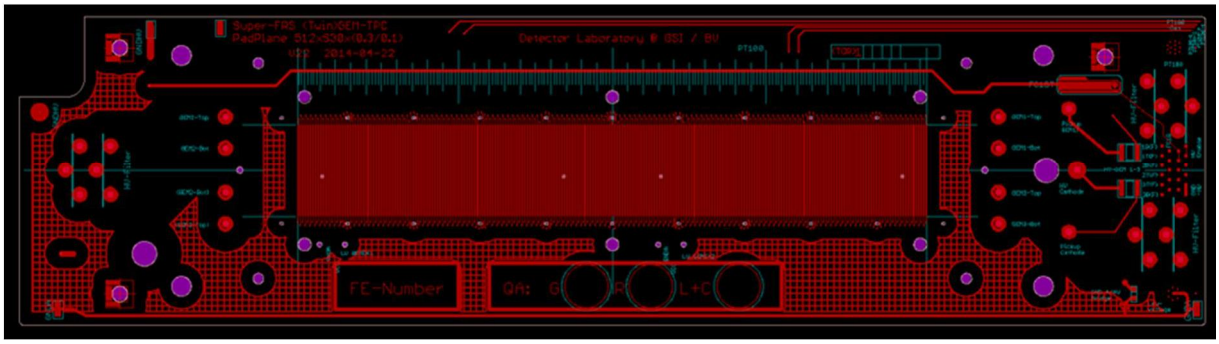

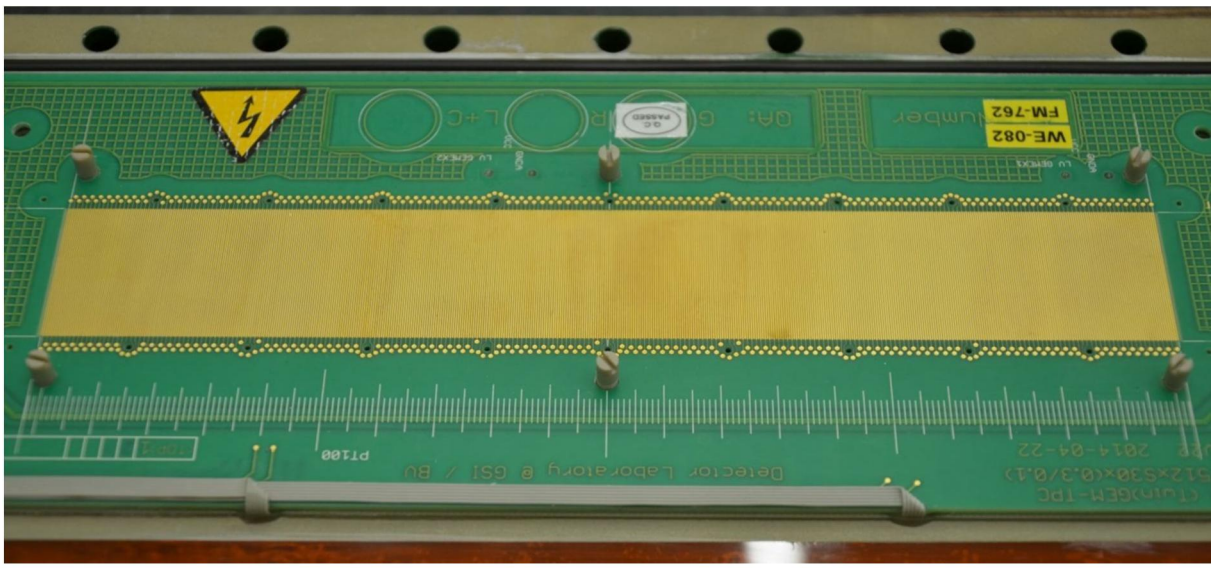

Figure 6.2: Cad design (upper part) and snap shot (lower part) of the surface of pad-plane of the Super-FRS GEM-TPC facing the gas volume. The inner 'active' area is patterned with 512 strip-type electrodes.

Fig. 6.3 shows a shot of the strip-type electrodes forming the read-out structure on the pad-plane of the Super-FRS GEM-TPC. The inner 'active' parts of the electrodes are 30 mm in length and 0.25 mm in width, the gap between neighboring pads is 0.15 mm and the pitch is 0.4 mm.

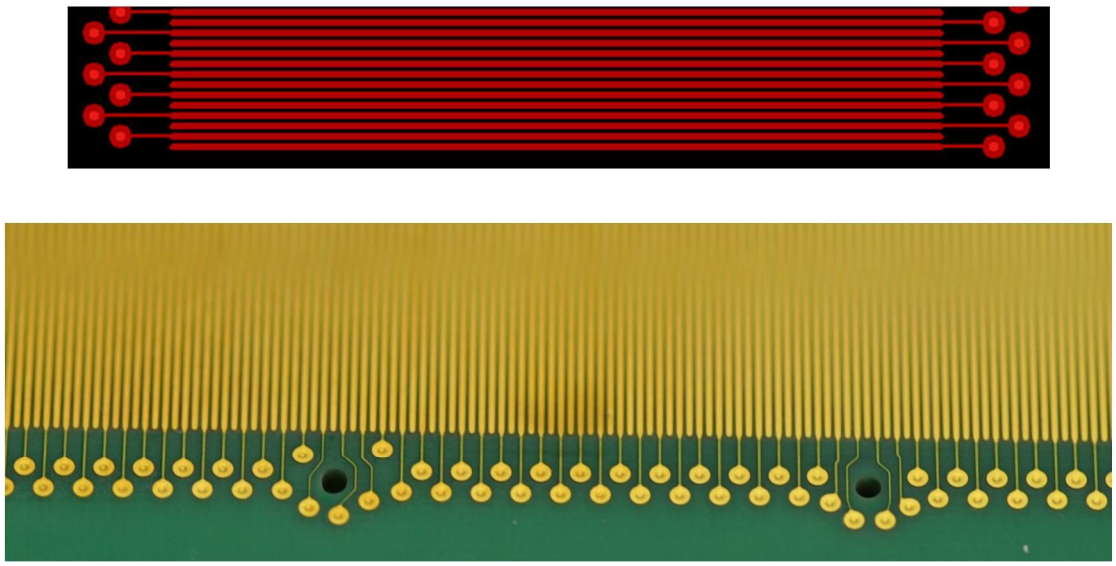

Figure 6.3: : CAD design (upper part) and snap shot (lower part) of the strip-type electrodes forming the read-out structure on the pad-plane of the Super-FRS GEM-TPC. The inner 'active' parts of the electrodes are 30 mm in length and 0.25 mm in width, the gap between neighboring pads is 0.15 mm and the pitch is 0.4 mm.

Fig. 6.4 shows a snap shot of the inner routing structures of pad-plane of the Super-FRS GEM-TPC. Gas-tightness of the PCB is assured using a 6-layer multi-layer design and by plugging the respective (blind and buried) through-holes. Realizing an appropriate high density (100 µm)

routing, an optimum (minimal) spread of routing length for all 512 signals has been achieved, minimizing the spread of the respective capacities.

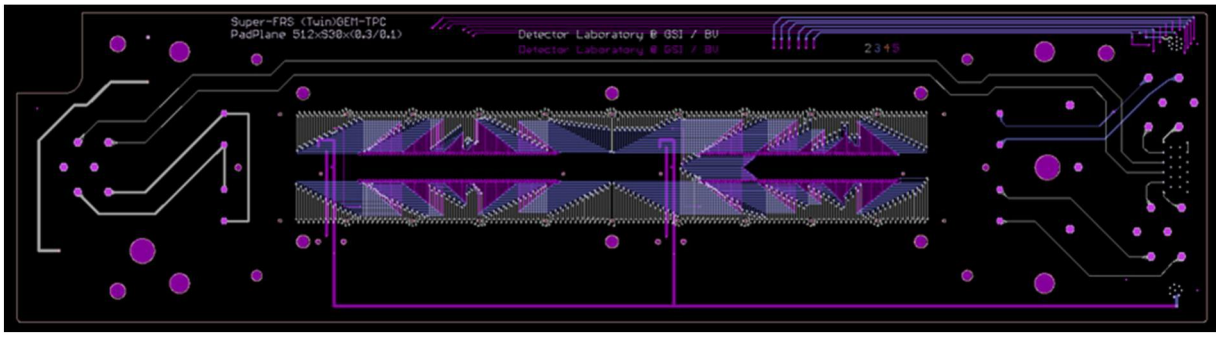

Figure 6.4: Snap shot of the inner routing structures of pad-plane of the Super-FRS GEM-TPC.

Great care has been taken to allow high-voltage routing through the pad-plane PCB by selecting the appropriate materials and layer stacking and designing sufficient insulation distances. An acceptance test applying 6 kV to all HV routes is part of the quality assurance procedure of the pad-plane PCB.

Connection to the supplies hardware outside of the detector is provided via a 22 pin REDEL connector allowing a 1:1 connection to e.g. a HVGEM module [ref]. Separate SHV connectors are used for the biasing of the 1st-strip of the field cage as well as for the cathode high-voltage.

The top/bottom contact-flaps of the 3 GEMs in the GEM-stack (see Fig. 6.11 and 6.12) are screwed directly to respective contact points on the pad-plane PCB.

Figure 6.5 displays a snap shot of the surface of the pad-plane of the Super-FRS GEM-TPC facing the ambient surrounding. The 512 electrodes on the front-surface are internally routed to two SAMTEC 300-pin high-density connectors (0.5mm pitch) each connecting 256 pads.

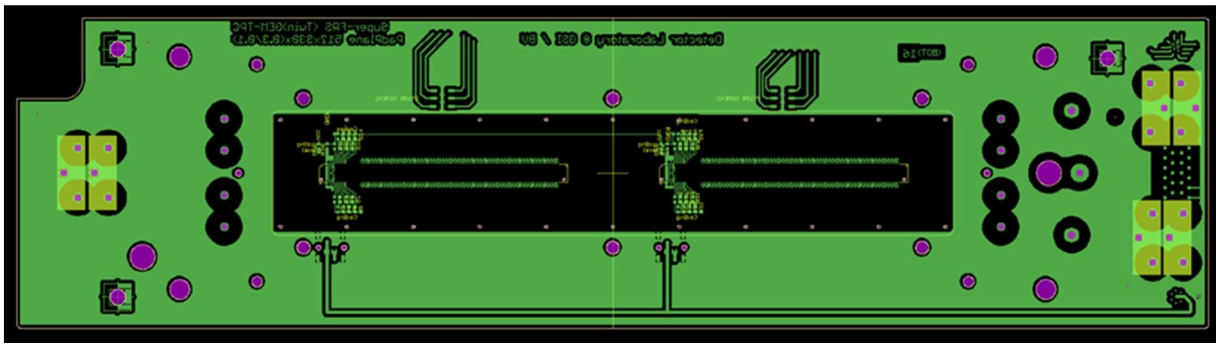

Figure 6.5: Snap shot of the back-side of the pad-plane of the Super-FRS GEM-TPC. The 512 electrodes on the front-surface are internally routed to two SAMTEC 300-pin high-density connectors each connecting 256 pads.

Several options for the powering of the read-out electronics sourced by a single input line have been realized on the pad-plane PCB for test purpose:

a) Direct powering of each front-end board via the respective SAMTEC ‘BTH’-type connector,

b) Split powering of the respective front-end boards via ERNI ‘mini-bridge’ type connectors,

c) External powering via the GEMCON PCB externally interconnecting the two front-end boards (not shown here).

6.2. HV filtering

High-voltage supply to the detectors usually is provided over large distances via long cables. In some cases it is advisable to implement filters directly in front of the device in order to get rid of electro-magnetic disturbances and to stabilize the electrical field in the field-cages. For this purpose sets of appropriate filters have been produced. The schematic applied is shown in Figure 6.6 exemplary for the supplies of GEM-foil no.1.

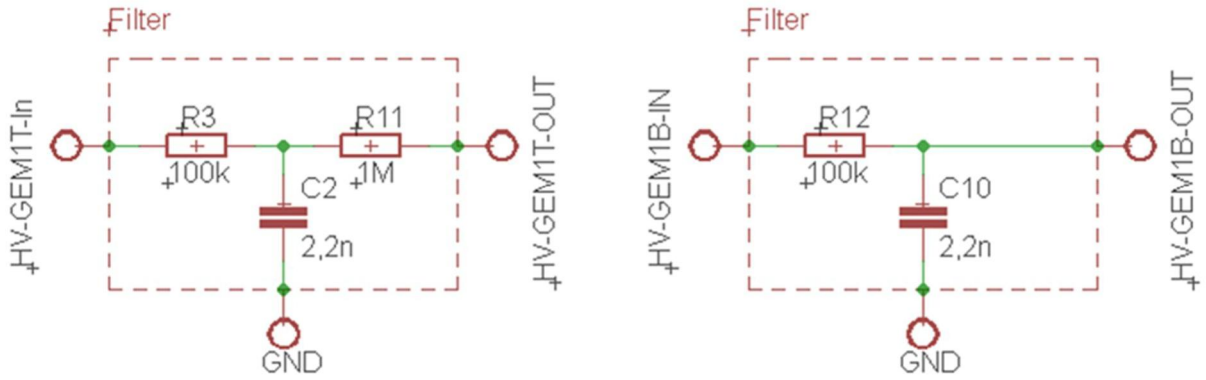

Figure 6.6: Electrical schematics used for the HV filters here exemplary showing connections to the top (T) and bottom (B) surfaces of GEM no. 1.

Fig. 6.7 shows a picture of two sets of high-voltage filters employed to filter the bias voltages for the GEM-foils. Before and after potting the filters have been tested for their high-voltage stability up to 10 kV. Nevertheless, the nominal operation voltage should not exceed 5.5 kV on long term cue to the ratings of some of its components.

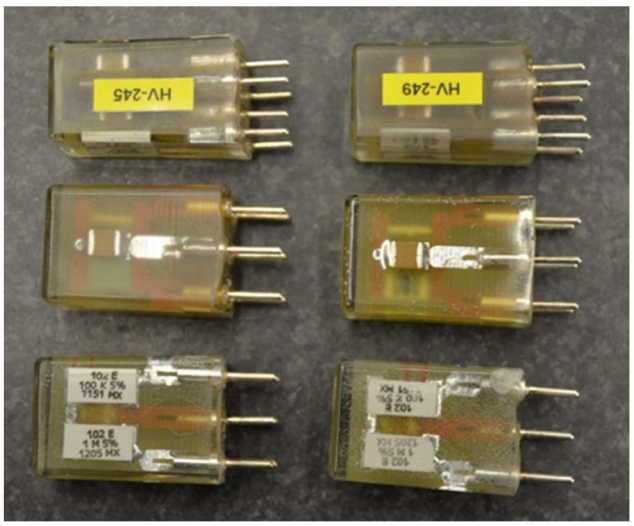

Figure 6.7: Picture of two complete sets of high-voltage filters employed to filter the bias voltages for the GEM-foils.

Their position inside the detectors vessel has been chosen as close as possible to the GEM-stacks in order to provide best possible filtering; an overview on the placement is given in Figure 6.8.

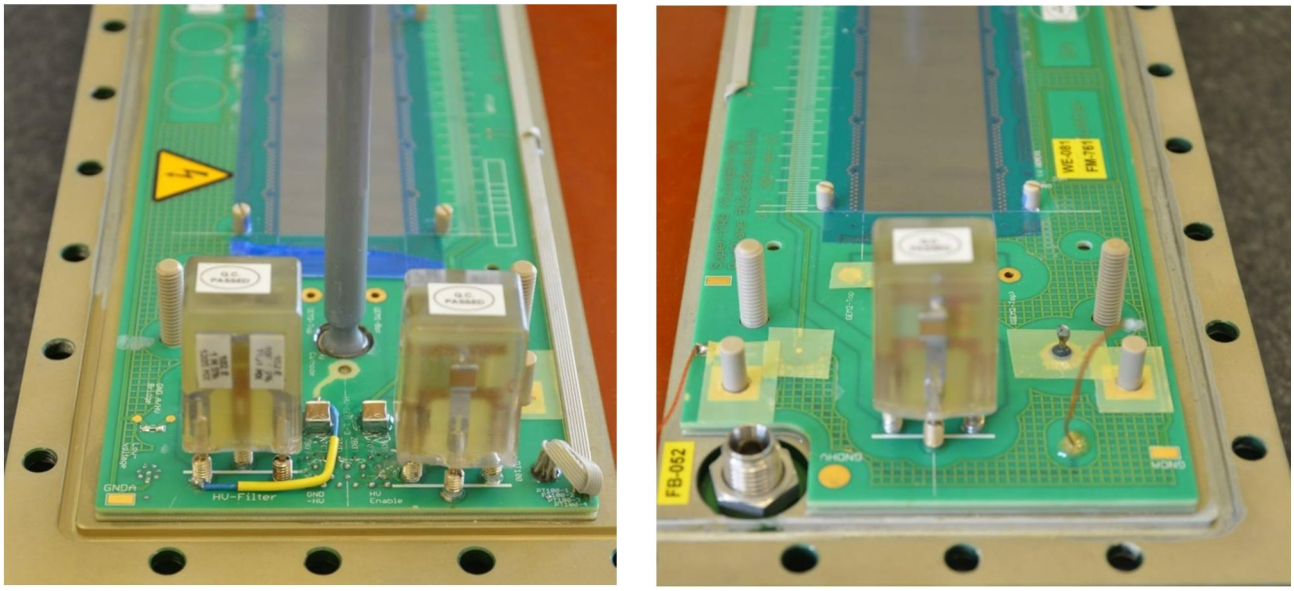

Figure 6.8: Picture of two complete sets of high-voltage filters employed to filter the bias voltages for the GEM-foils.

6.3. Interface to readout electronics

Interfacing to the read-out electronics flanged to the panel and the cooler setup, respectively, is provided via high-density fine-pitch connectors of type SAMTEC BTH-150-01-L-D-A-X which offers up to 300 pins, 256 being used for signal transfer. The rest of the pins have been reserved for powering as well as the implementation of additional functionalities like e.g. unambiguous coding, steering and control of analogue pre-attenuators etc. The actual pin assignment can be found in Table 6.1.

Assignment for Super- FRS (Twin) GEM-TPC					
Pin-Index	**Connector-Pin**		**Signal**	**Direction**	**Description**
1	1	2	GND-D	Supply	(Digital) Ground
2	3	4	VCC		
3	5	6	GND-D		+3,3V / +5V
4	7	8	VCC		
5	9	10	GND-D		
6	11	12	SlotNo Bit0	Out	Coded on PadPlane
7	13	14	SlotNo Bit1		
8	15	16	SlotNo Bit2		
9	17	18	SlotNo Bit3		
10	19	20	SlotNo Bit4		
11	21	22	SlotNo Bit5		
12	23	24	SlotNo Bit6		
13	25	26	SlotNo Bit7		
14	27	28	ChipID Bit0 / VCC	Reserved (e.g. Pre-Divider - Absorber …)	Coded on FE-Board
15	29	30	ChipID Bit1 / VCC		
16	31	32	ChipID Bit2 / Out C1		
17	33	34	ChipID Bit3 / TDB LF		
18	35	36	ChipID Bit4 / TCK CLK		
19	37	38	ChipID Bit5 / TMS Data		
20	39	40	ChipID Bit6 / TDA C16		
21	41	42	GND-A	Supply	(Analog) Ground
22	43	44	GND-A		
23	45	46	XYTER-Channel 1	IN	Pads on PadPlane
…	…		…		
150	299	300	XYTER-Channel 256	IN	

Table 6.1: Pin assignment of the SAMTEC BTH-150.

A picture of the two adjacent SAMTEC connects mounted on the pad-plane PCB glued to the read-out flange is shown in Figure 6.9. Channel counting is continuously 1-256, 257-512 following the unique scheme shown in Table 6.1.

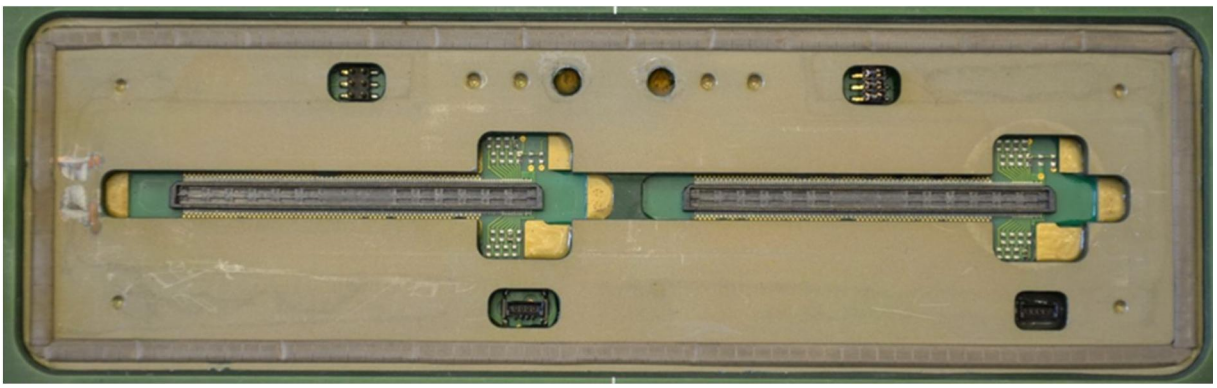

Figure 6.9: Picture of two adjacent high-density read-out connectors mounted on the back-side of the Pad-plane PCB (the copper cooler has been removed for that purpose).

6.4. GEM stack

The GEM-foils employed in this project so far were produced by CERN. Their active area is of square shape: 210 x 28 mm^2. A set of three framed GEM-foils are stacked in a 'typical' 2-2-2 (mm) arrangement which is somehow a 'standard' in the field for historical reasons. A picture of such a stack arrangement with so far un-trimmed connector 'flaps' is given in Figure 6.10.

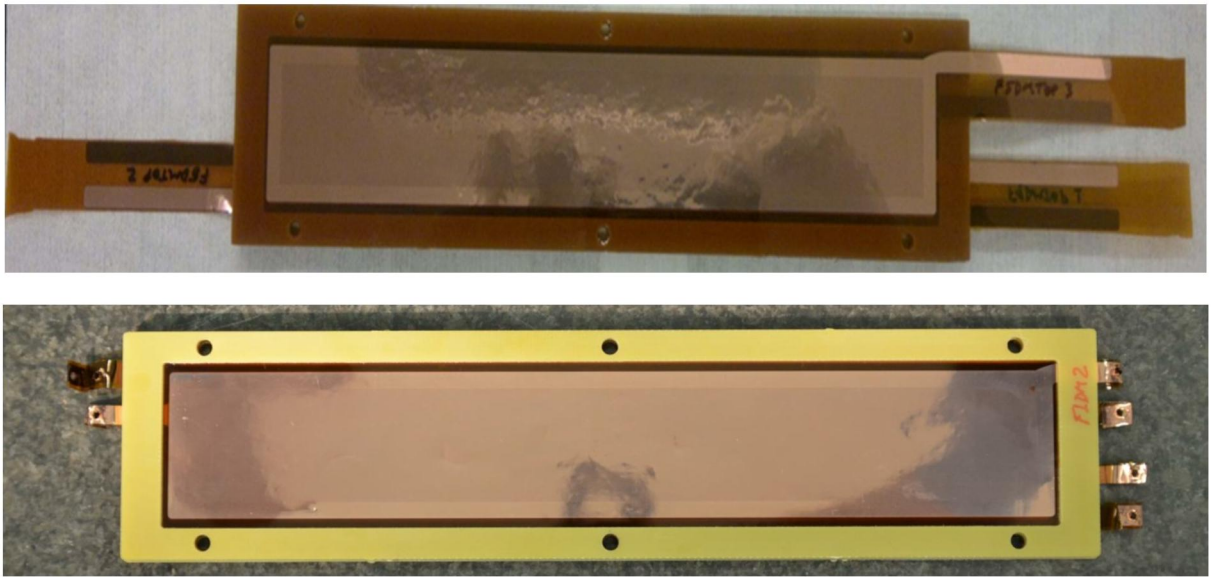

Figure 6.10: Picture of a set of three framed GEM-foils forming the amplification stage of a single compartment of the Super-FRS TwinGEM-TPC from te top side with uncut flaps (upper part) and from the bottom side with flaps 'ready-to-mount' (lower part).

The 'flaps' are used to lead out the electrical signal of each surface of the various GEM-foils. They are directly screwed to corresponding pads on the pad-plane as can be seen in Figure 6.11 and 6.12.

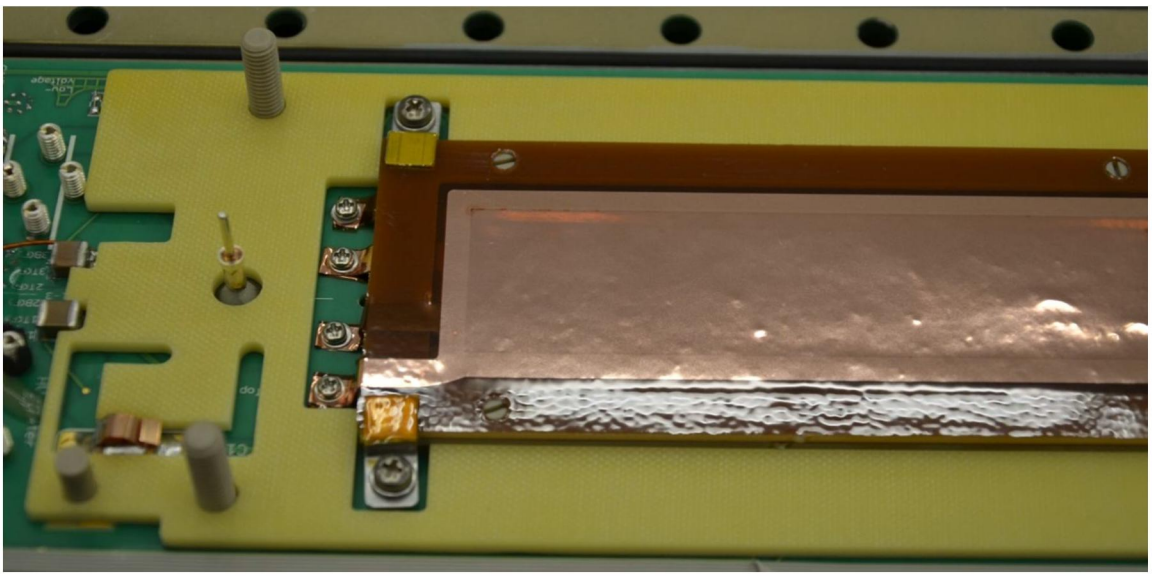

Figure 6.11: Picture of a GEM-stack screwed to the pad-plane.

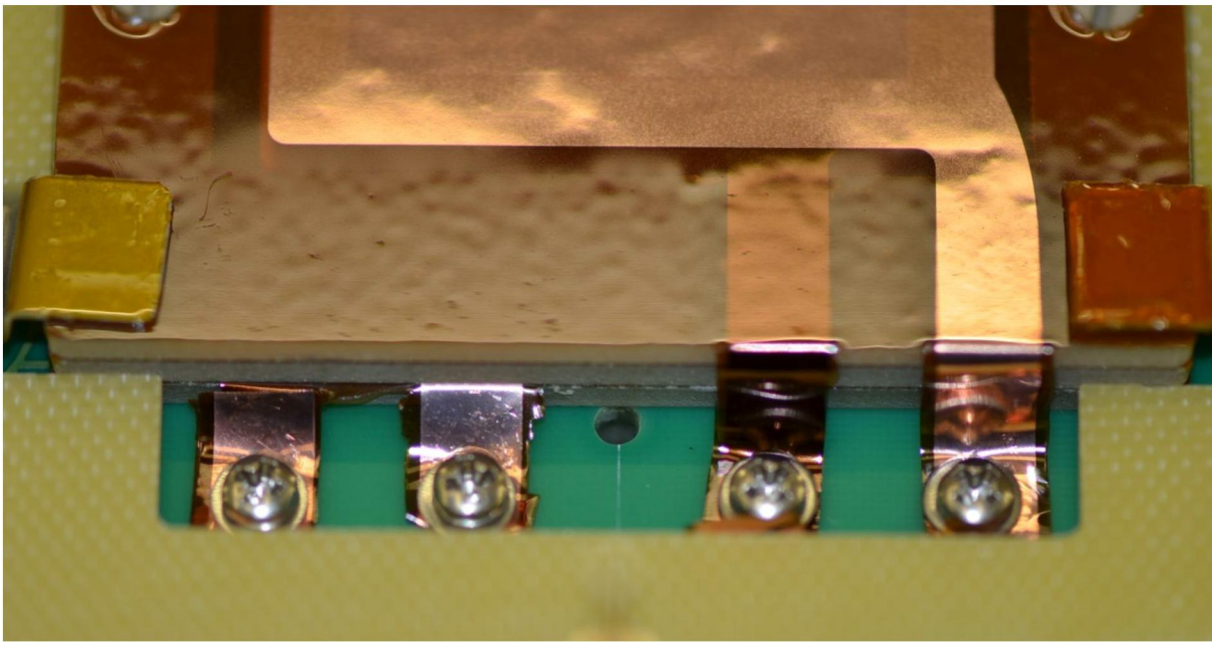

Figure 6.12: Picture of the flaps of the GEM-stack screwed to the pad-plane.

7. GEM stack quality assurance and tests

Special care is taken after the assembly of the whole detector to assure a leak-less operation. For that purpose a slight overpressure (100 mbar) is applied and its stability over several hours is checked. In addition, the gas purity is monitored. Usually the oxygen level is below 6 ppm and the water content in the order of 200 ppm for a freshly mounted detector.

The isolation stability of the high-voltage lines is tested by measuring the resistance between the routes leading to the GEMs as well as the respective value with respect to Ground/GND of the panel a/o housing vessel. Accepted levels are in the order of 10 TΩ for $R_{GEM-GEM}$ and 100 TΩ for $R_{GEM-GND}$.

7.1. GEM foil quality assurances

The proper selection of the GEM foils to be used into the GEM stack of a GEM based TPC for the Super-FRS is of major importance [6].

Many experiments has been used GEM detectors and a set of procedures has been stablished in order to guarantee the proper selection of the GEM foils to be used in the GEM stack of a GEM based TPC. The first experiment to use large GEM foils was COMPASS [7], followed there were many other experiments LHCb [8], PHENIX **Error! Reference source not found.**, TOTEM [5] and more recently for the upgrade of the ALICE TPC [6].

This chapter we will cover the requirements needed for transportation, electrical and optical checks and its performance uniformity. In order to minimize the risk of failure and provide long term operation of the chambers a methodology has been developed and follow we will discuss each of the steps with its limits of acceptance.

7.2. Visual inspection

As a first step upon arrival of the GEM foils a visual inspection is carried out, this procedure will serve as a first screening procedure, because it will allow us to find large side scratches, regions with defects due to under or over etching and residual deposition in the GEM foils. Below is the picture of a single foil with five GEM foils on it, this type of GEM foils has been used for the twin GEM-TPC, called HGB4.

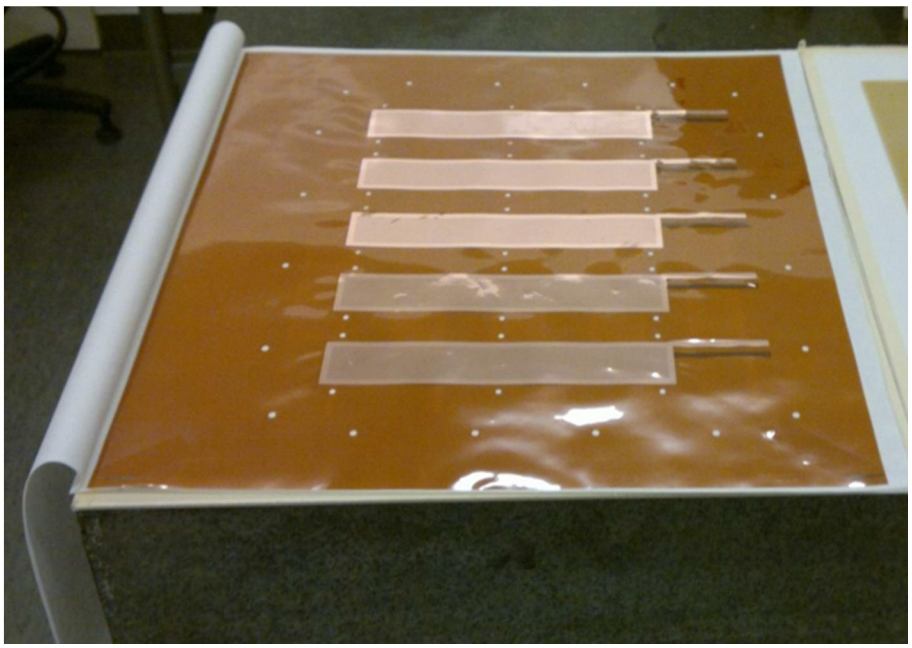

Figure 7.1: GEM foils for the twin GEM-TPC called HGB4.

One major defect that can be identify during this inspection will be the presence of wrinkles on the GEM foil, this defect is important to quantify, since depending on the dimensions one cannot expect to remove it by stretching the foil. In addition to that wrinkles could be potentially point out to possible defects between Copper and Kapton interface. Therefore a GEM foils with very smooth surface will be preferable pass this step.

7.3. Electrical characterization

The electrical characterization of the GEM foils is the next step in the process of accepting or rejecting a GEM foil. The measuring of the leakage current in particular for each sector can show how stable it can withstand a potential difference across the two sides. These electrodes are located on top and bottom of the insulator Kapton insulator layer. The test is carry out in dry atmosphere in order to avoid breakdowns provoked by the water contend in air and thus directly test the insulator quality. One of the most common gases used to get a dry atmosphere is Nitrogen and therefore flushing the vessel prior to the test is mandatory. The setup used for the leakage current measurement is shown in Figure 7.2. The components of this setup are: a desiccator with a gas flow meter, an electrometer, a voltage source and a computer for control the ramping of voltages and store the current measurements. The procedure consists in applying a voltage difference between the top and bottom electrode from 100 V up to 500 V in steps of 100 V and constantly monitoring the current circulating between the electrodes. Tis current is monitored and if the value is <0.5 nA the next ramping step is performed, when the maximum voltage of 500 V is reached, then current is monitored for 30 min, in the case that the current is <0.1 nA the GEM foil will be accepted for the next check otherwise it will be undergo either thermal treatment or send back to the producer for further cleaning.

Figure 7.2: Leakage current measurement setup.

A typical behavior of the leakage current measurement is shown in Fig. 7.3. It can be seen that current is well below the acceptance limit, thus such a foil is accepted. However on the Fig. 7.4 one can see the behavior of another type of foils when during the initial ramping of the HV the GEM foil shows typical operation, but after sometime it experienced several sparks and after flushing the vessel, the leakage current move back to normal.

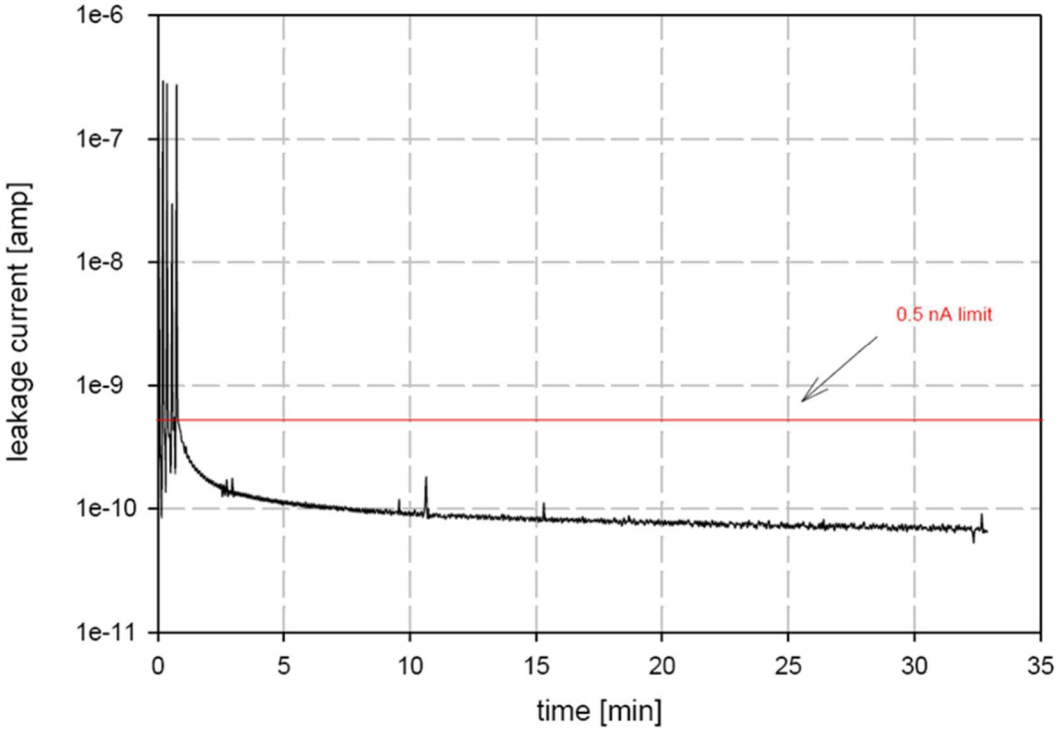

Figure 7.3: Leakage current results from a good working GEM foil, the evolution of this step in the characterization shows that the GEM foil performs well and it is accepted. The acceptance criteria is a leakage current of < 0.5 nA for 30 min at 500 V in dry atmosphere.

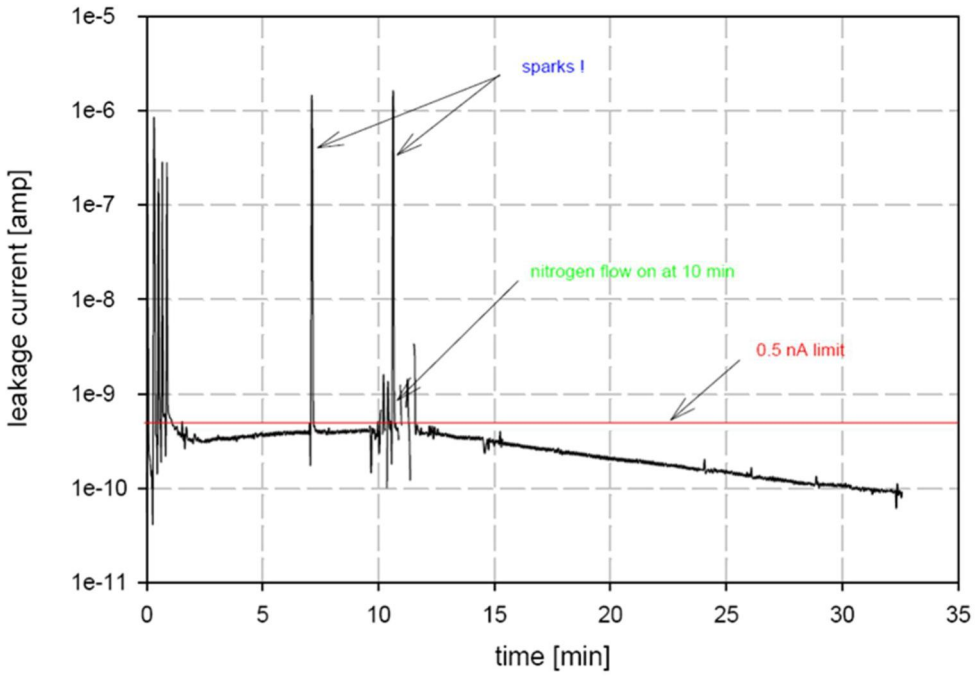

Figure 7.4: Leakage current results from a recovered GEM foil

7.4. Optical characterization

After a foil has passed the coarse visual inspection and the static electrical quality assurance testing, it is subjected to precision optical inspection using a high resolution scanning system. In this way the geometrical characteristics of the GEM foil can be studied. In particular, the distributions of inner and outer hole diameters and the hole pitch for both sides of the foil are measured. It is well known that a variation of the inner hole diameter and the ratio of the inner outer hole diameters causes a variation of the intrinsic gain of the foil. The dispersion of the distributions can be taken as a quantitative indicator of the general foil uniformity. Foils not meeting the specifications over the full surface (i.e. copper hole diameter typically (70 ± 5) µm, polyimide hole diameter typically (55 ± 5) µm) are rejected. In addition, the method is suited to identify smaller defects which were not detected in the first visual inspection step. Defects in the form of under- or over-etched areas in the foils can occur during the manufacturing process. Other type of defects may come in the form of chemical residues from the production process, or dust attached to the foil, very large holes, missing holes, etc. All of them may cause operational instabilities. The setup used for this purpose is based on a back-illuminated light table with area (100x100) cm^2. In Figure 7.5 the scanner used for this optical characterization is shown [25]. A 9Megapixel camera with a single pixel size of 1.75 μm^2 is mounted on an x-y positioning system above the light table. The optical system has a resolution of 144 light points per mm and a field of view (single image) of (6.1x4.6) mm^2. After compression, the total image size is about 20 MBytes. Up to 500 individual images are required to cover the full active area on both sides.

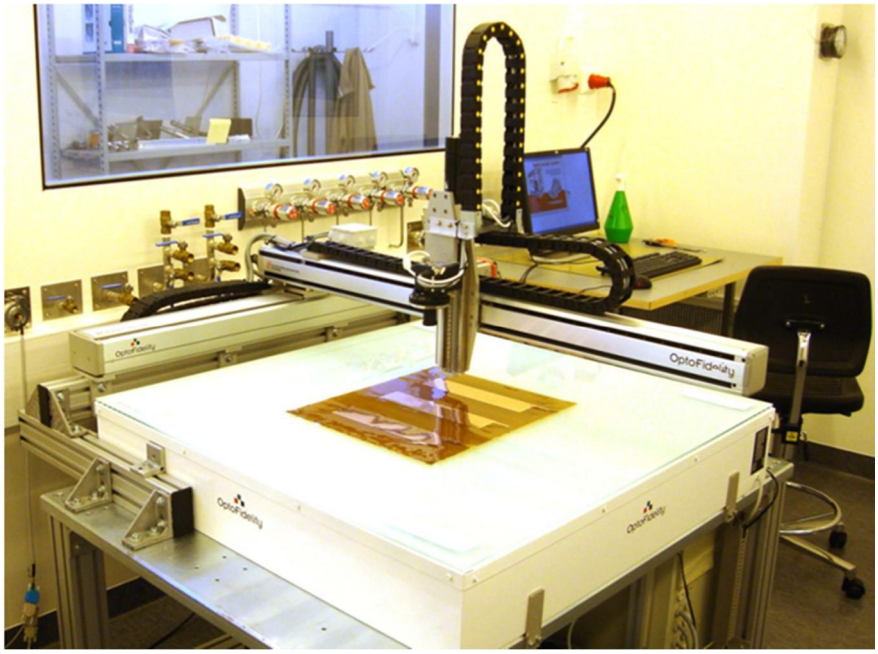

Figure 7.5: Setup of the high resolution scanning system.

During the scanning procedure the diameters of inner and outer holes, the pitch between holes and their shape are recorded. Distributions of the diameter, the width of the polyimide rim (the distance between the border of the outer and inner holes), and the pitch are shown in Figure 7.6. Parameters describing the shape of the hole are obtained from an ellipse interpolation with a sigma of about 0.84 µm for the inner hole.

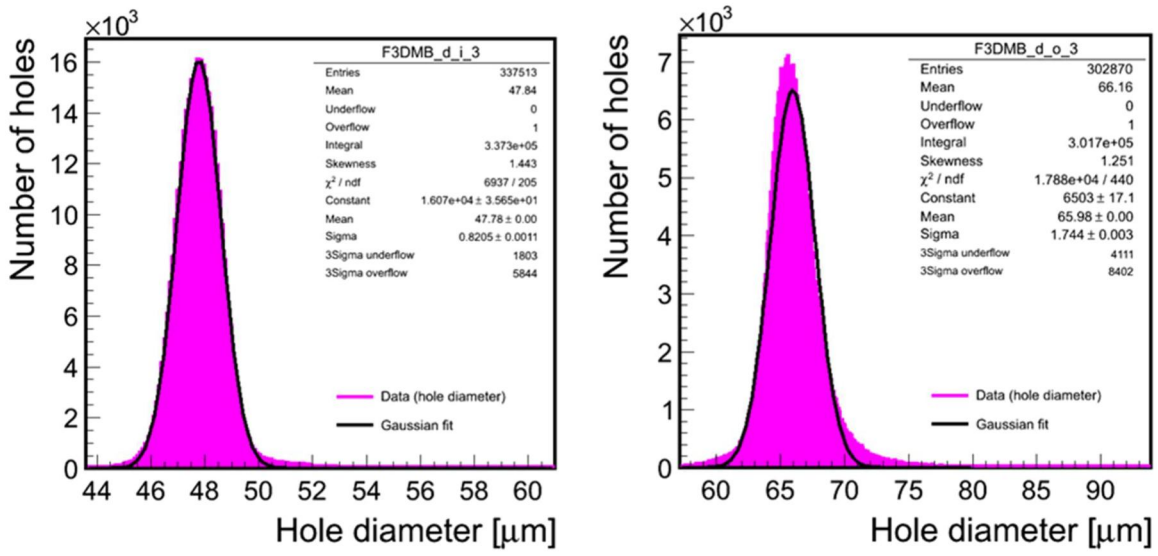

Figure 7.6: Distribution of the hole diameter for a FRS foil. On the left side the inner hole diameter and on the right the outer correspondently.

A two-dimensional map of the GEM foil characteristics is used to visualize the uniformity of measured parameters as a function of position on the foil. Fig. 7.9 shows an example of the spatial variation of the diameters of the inner and the outer holes. Here, the diameters of holes are averaged over an area of 2.5 mm^2 x 2 mm^2. Maps such as these can be used during assembly of the GEM stack to avoid accumulation of unwanted features in similar positions over the stack area.

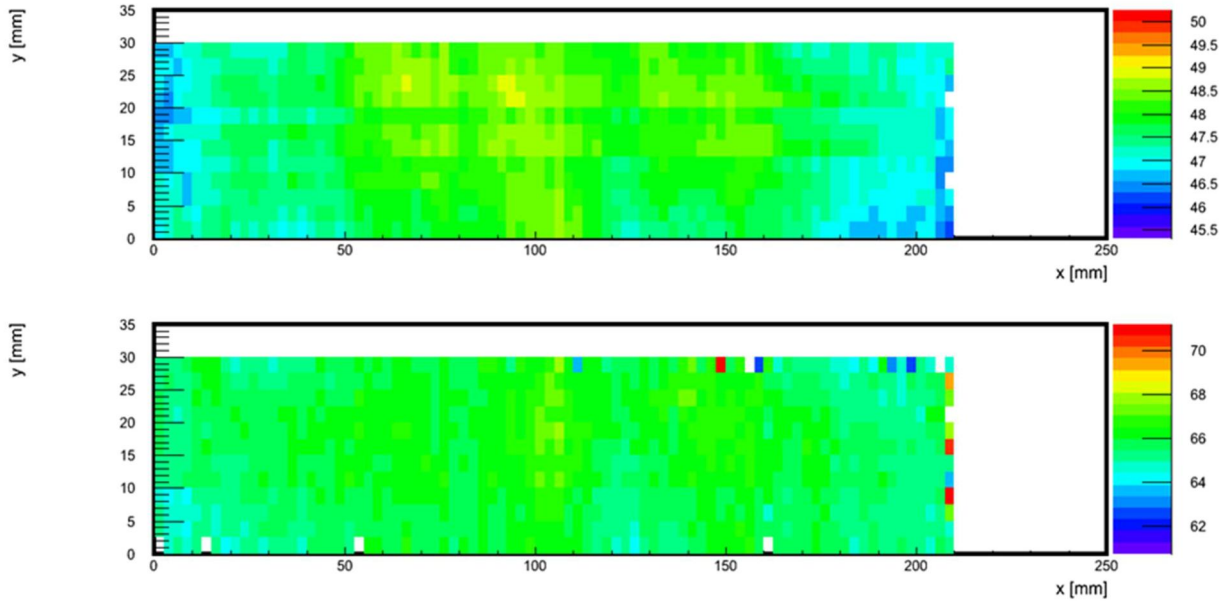

Figure 7.7: Map for the distribution of the hole diameter for a FRS foil. On the top for the inner hole diameter and on the bottom for the outer correspondently.

7.5. Gain uniformity measurements

An acceptable performance of a GEM stack of the GEM-TPC partly will be determined by the uniformity of the gain across the whole active area, therefore a mapping of the gain of each GEM stack need to be done. This mapping will allow us to find none uniformity of the gain across the whole active are and provide all the necessary information either for the final acceptance or for its rejection. In the case that the gain variation of the foil will be inside the acceptance limit of about 7% then the this will be ready to be mounted on a the chamber of the GEM-TPC. The test bench for the measurement of the gain is shown in Fig. 7.8.

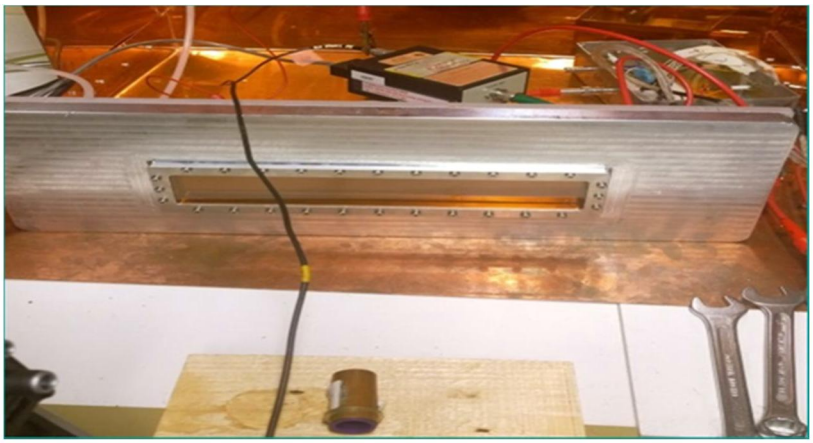

Figure 7.8: Schematics of the setup for the gain mapping.

The gain calibration for the GEM stack in gas P10 is shown in the Fig. 7.9, it can be seen that the gain is linear. There are plans to provide the gain mapping in one coordinate along the beam and a setup is now in construction using the scalable readout system and the APV25 hybrids.

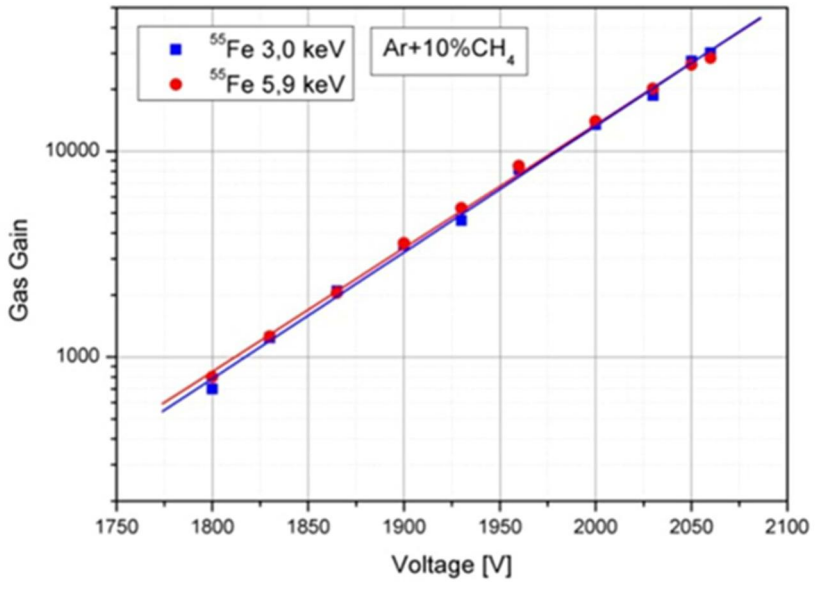

Figure 7.9: The gain verus the high voltage at the divider is shown for P10

8. Field cage quality assurance

It is the main task of a field cage employed in a magnetic spectrometer such as the future Super-FRS to define and enclose a volume of constant / very homogeneous electrical field without unacceptable interference with the particles traversing this so called active drift volume. To serve that purpose, several requirements apply.

- In a high-rate environment such as present at several places in the future Super-FRS, with very heavy particles impinging, the materials in use should be radiation hard to withstand several years of operation.
- The resolving power properties of the spectrometer should not be spoiled by changing the properties of traversing particles, resp. 'beam quality', e.g. by changing its distribution in
    - isotopic composition (Z,A) thus avoiding nuclear reactions
    - charge state Z_{eff} due to charge pickup
    - the 'emittance' (directions transversal and longitudinal to the beam) by adding straggling contributions with respect to
        - the geometry of particle distribution
        - the velocity a/o momentum of the beams particles
- All mechanical key-values of the materials itself as well as their geometry has to be stable over long-time for a high-precision operation.
- The field-defining surfaces have to be geometrically flat since any structure in the geometry defining the local electrical potential will directly spoil its homogeneity. Considering foils in general, this also has implications of their material properties with respect to the forces to be applied to kept thin materials flat.
- The whole unit has to be immune against external electro-magnetic interferences. Thus appropriate screening properties need to be considered.

These requirements call for a very thin, flat and mechanically stable and highly durable material with low-Z and low density and good homogeneity in all its properties.

One possible material which in general meets the above mentioned requirements is a foil made from polyimide. A 7.5 µm thick Kapton®-HN foil by DuPont with double-sided staggered/mirrored strip-wise aluminized layers forming equipotential areas have been chosen for the GEM-TPC for details).

The sequence of aluminized strips is impressed with continuously and stepwise changing electrical potentials provided by a chain of SMD-type resistors mounted on a separate PCB.

Each field-cage assembly comprises a variety of parts which all together define and enclose a volume of constant electrical field:

1. Cathode plate
2. Skimmer / 1st-strip field terminator
3. Strip-line foil with resistor chain(s)

Several small pieces mechanically and electrically mount everything together

8.1. Cathode

The cathode plate is shown in Fig. 8.1. It is made from a 1.5 mm thick FR4 plate mounted on a 5 mm thick Stesalit 4412 / G10 backing which is providing appropriate stiffness and flatness as well as an integrated gas-distribution system.

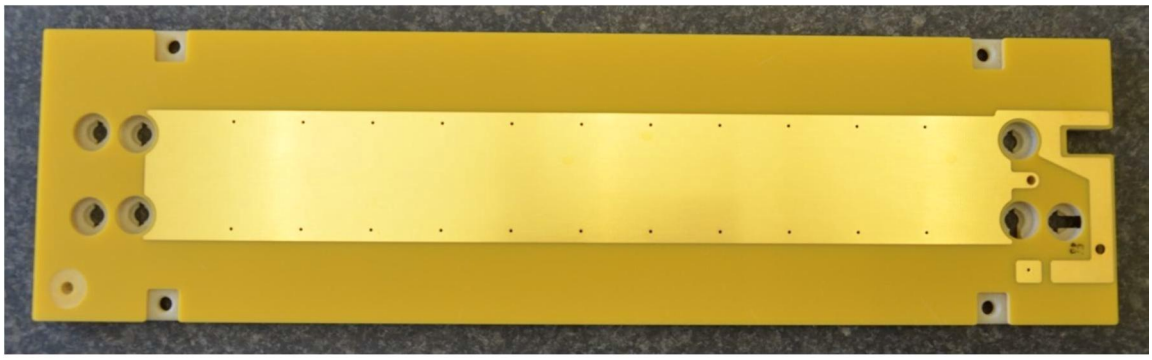

Figure 8.1: Picture of the cathode plate mounted on its backing.

8.2. Skimmer and field terminator

The field terminating plate is shown in Fig. 8.2. It is made from a 0.5 mm thick FR4 PCB and has been glued to a backing support made from 3.2 mm thick glass-fiber reinforced PEEK plate which is providing appropriate stiffness and flatness.

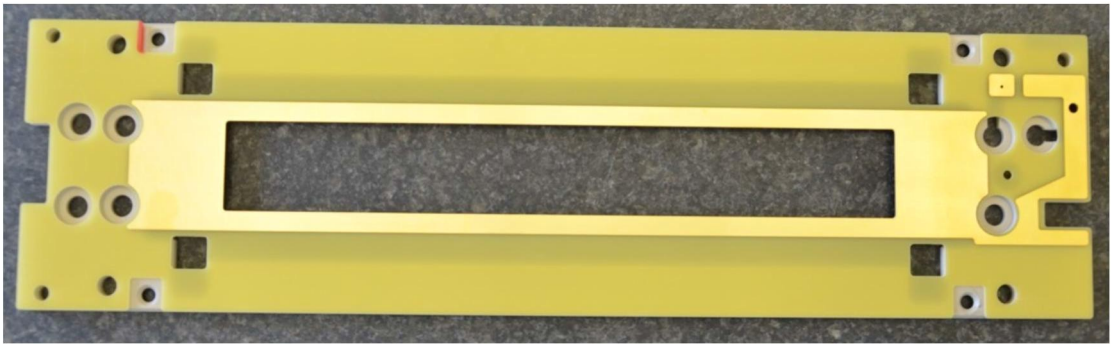

Figure 8.2: Picture of the field-terminating plate mounted on its backing.

This electrode is kept on the same electrical potential as the first strip of the strip-line foils of the field-cage. Its absolute value can be adjusted via a separately fed supply voltage to be identical to the top-surface of the first GEM foil facing the drift volume.

8.3. Field cage strip-line foil

In order to minimize the effect of the step-wise electrical gradient on the homogeneity of the electrical field enclosed in the drift volume, the structure has to be kept as small as possible. Obeying technical boundary conditions a strip width of 3 mm and a gap of 2 mm have been chosen. A picture of the foil is shown in Fig. 8.3).

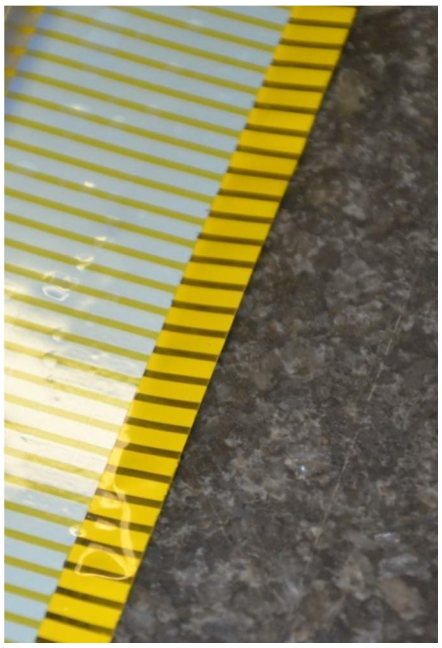

Figure 8.3: Picture of the field-cage strip-line foil, the staggered structure of the field defining aluminum stripes in the front as well as the mirror stripes on the back-side surface are clearly visible.

Choosing Aluminum of reasonable thickness (several 100 nm) as coating material for the strips preserves a reasonably low resistivity (and thus a voltage-drop) over the length of a strip.

Stretching of the foil is done using a system of bars in the edges of the active area. Allowing the walls of the field cage to be slightly larger than the copper-plated area of the GEMs ensures a nearly disturbance free drift in the active volume. This ensures a clean, undisturbed projection of a particles track to the subsequent pad-plane.

8.4. Field cage voltage divider

Two identical resistor dividers operated in parallel are mounted on both ends of the strip-line type field-cage foil. Choosing this double-sided ending splits the currents across the respective dividers into half, distributing power consumption and generated heat. A picture of these dividers is shown in Fig. 8.4.

Half of the resistor dividers have been equipped with 4x32 pcs ‘real’ high-voltage resistors SMD 1206 of 3.0 MΩ resistivity, providing excellent tolerance (0.1 %) and low TCR values (25-100 ppm/C). They sum up to a total mean resistivity across the mounted field cage of 24.79 ± 0.01 MΩ.

For comparison and evaluation, the other half was equipped with 4x32 pcs ‘standard’ type resistors SMD 1206 of 3.3 MΩ and 0.5 % tolerance (0.1% via selection) which are much cheaper. They sum up to a total mean resistivity of across the field cage of 27.72 ± 0.01 MΩ.

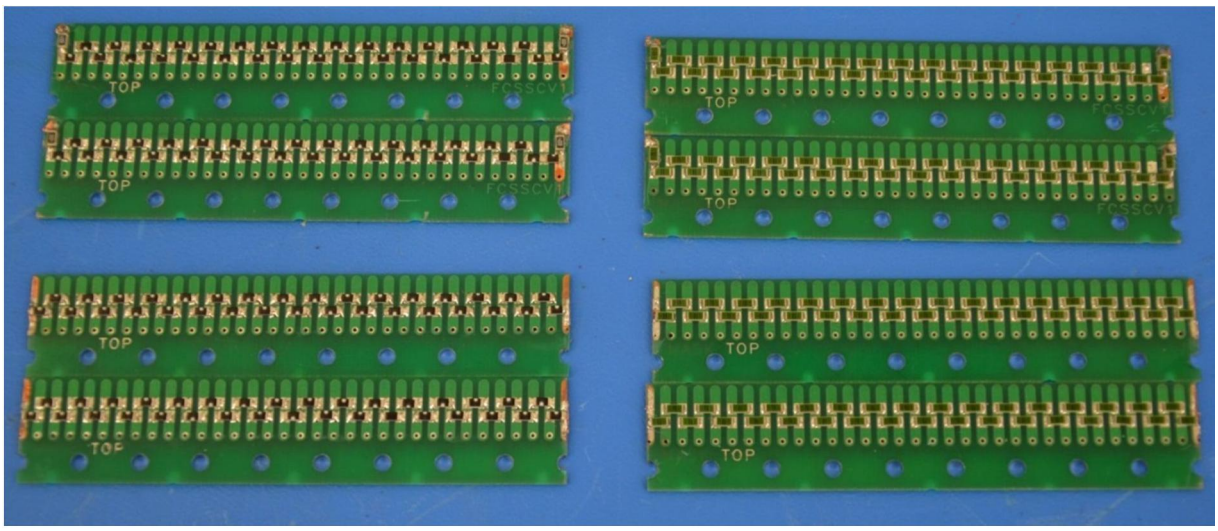

Figure 8.4: Picture of the resistor dividers for two identical field-cages in the 'Twin' configuration of the Super-FRS GEM-TPC. The left part shows the PCB with 'standard' resistors part-mounted, the right pair is equipped with 'high-precision high-voltage' type SMD resistors.

The full field-cage assembly is shown in Figs. 8.5 and 8.6. The latter also shows the double–sided metallized foil mounted in between the two field cage compartments of the 'Twin' configuration for screening purpose.

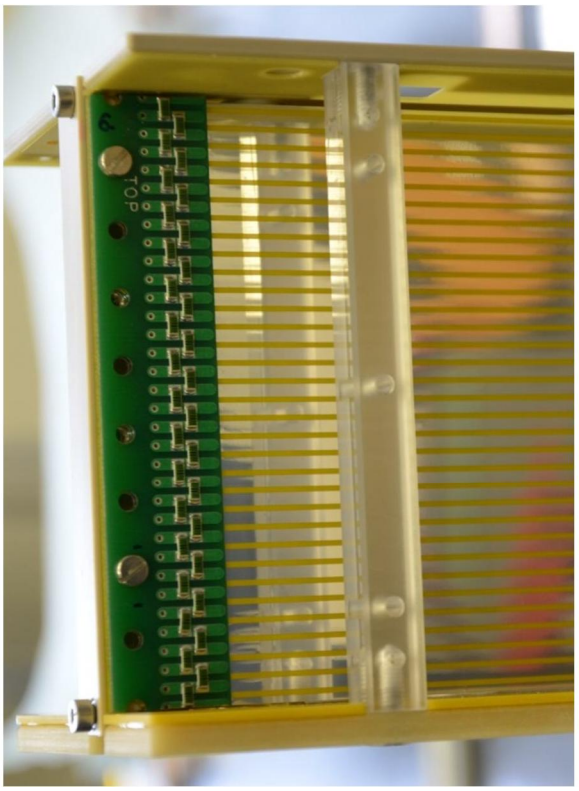

Figure 8.5: Picture of one of the two field-cages of the Super-FRS TwinGEM-TPC.

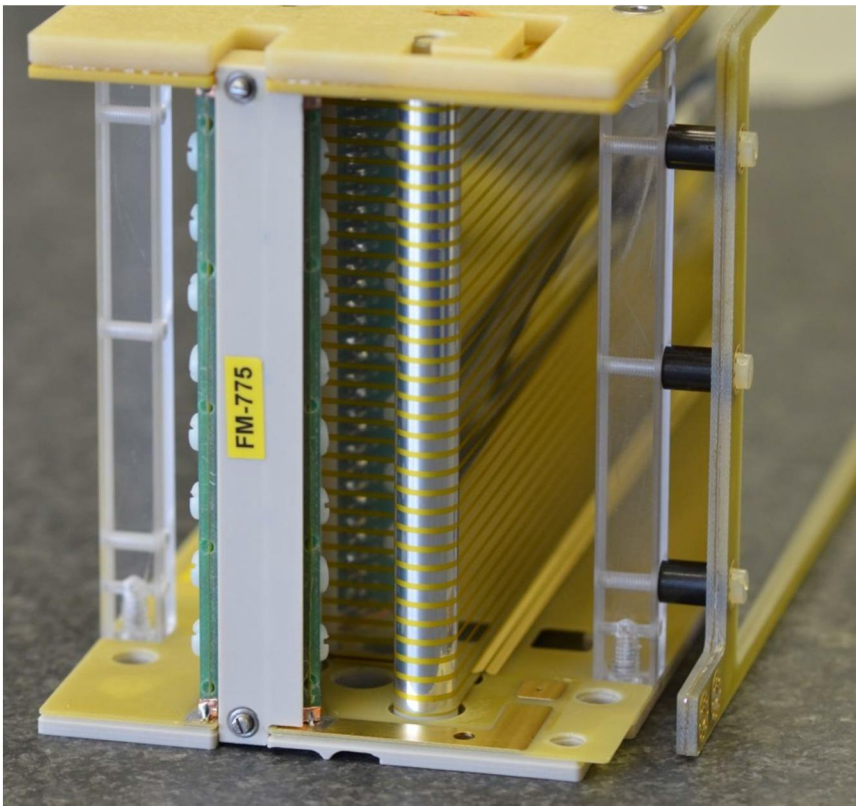

Figure 8.6: Picture of one of the two field-cages of the Super-FRS TwinGEM-TPC. Two identical resistor dividers operated in parallel are mounted on both ends of the strip-line type filed cage foil. The double–sided metallized foil mounted in between the two field cage compartments of the 'Twin' configuration for screening purpose is also visible.

8.5. Assembling and mounting

The whole design of the detector is highly modular and as compact as possible in order to minimize the overall space requirements in view of the later conditions to be faced at the Super-FRS. During installation only very little manual interactions are required to potentially exchange faulty parts. Except for the flaps of the framed GEM-foils in the GEM-stack no electrical connection has to be done explicitly and only one fluid connector (gas out) needs to be joined.

The following main elements can be identified which need to be mounted successively in order to assemble a single autonomously operating GEM-TPC as shown in Fig. 8.7:

1. Detector panel-flange integrating flange, pad-plane, cooler and read-out electronics
2. GEM-stack
3. HV-filters
4. Field-defining system enclosing the drift-volume consisting of Cathode, Strip-line field-cage foil, skimmer

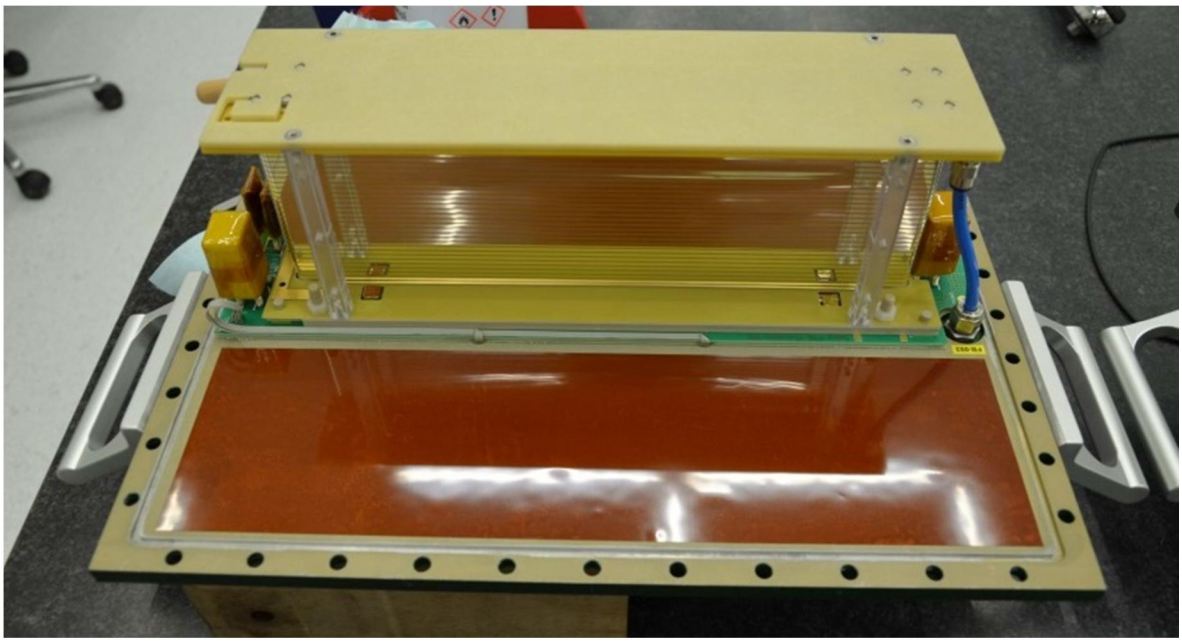

Figure 8.7: Picture of one half of the TwinGEM-TPC mounted on its panel.

Having two of those sets assembled, the two compartments can be joined with the detector housing / vessel as shown in Fig. 8.8. As can be seen easily, isolation distances with respect to the surrounding housing on electrical 'Ground' potential are kept to a minimum in order to minimize the overall space requirements. In the current design this is limiting the maximum operation voltage to 6 kV for a safe spark-free operation.

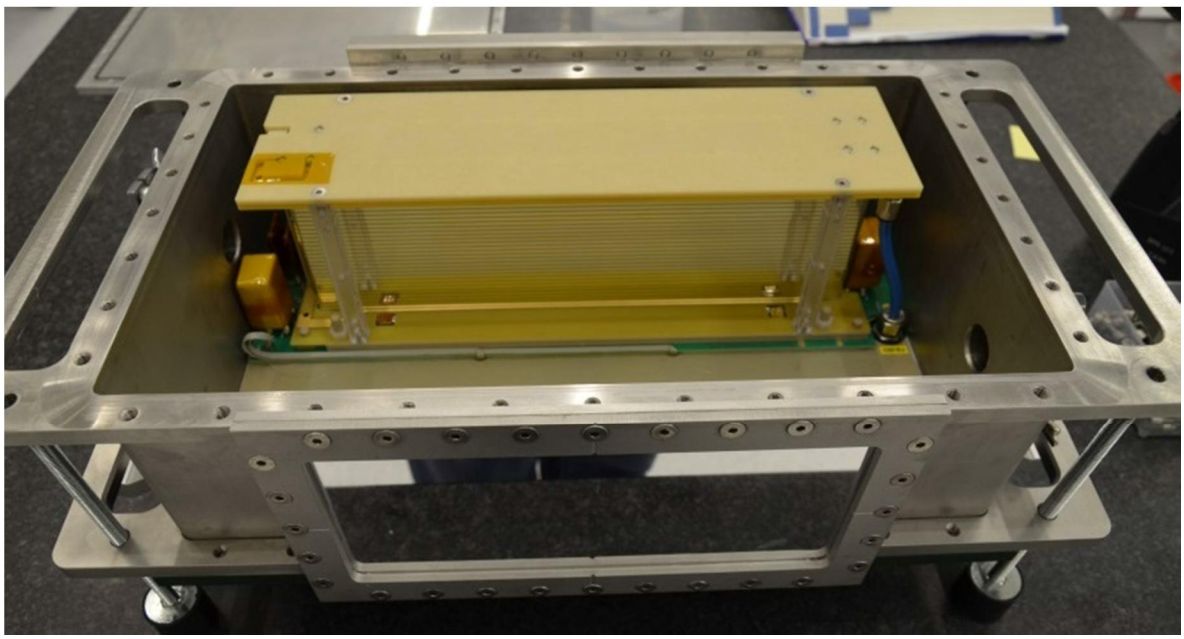

Figure 8.8: Picture of the first of two compartments of the TwinGEM-TPC installed inside the stainless steel vessel.

8.6. Field cage quality assurances

In order not to deteriorate/vary the equipotential levels along the strips by voltage drops a reasonably high conductivity of the structures of the field-defining system have to be assured. This is subject to QA processes.

Moreover a stable voltage drop across the structures over several years of operation require long-term stability of the resistors of the voltage divider employed as well as of the interface contacts.

8.6.1. Foil inspection

The foil has been inspected visually using a digital microscope for any apparent damages or interruptions in the metallization or shorts between neighboring strips. Faulty parts have been rejected.

8.6.2. Electrical tests

Electrically the appropriate insulation between neighboring strips as well as shorts (e.g. through pin holes) between back- and front-side strips have been tested prior to mounting of the resistor-divider PCBs. Faulty parts have been rejected.

The whole field-cage setup is tested for spark-free operation up to 5.5 kV in Ar/CO_2 (80/20 vol.-%) detector gas.

8.6.3. Performance stability

Performance stability will be checked in the future, especially for the parts which are potential subjects to aging effects under high-dose irradiations. This refers e.g. to

- the mechanical and electrical properties of the polyimide base-material of the field-cage foils,
- the durability of the aluminum metallization,
- the absolute and relative value of the resistivity of the SMD-type resistors (of various types) of the voltage divider across the field cage and
- the contact resistivity between the respective parts.

9. Front-end electronics

The design of the readout electronics is driven by the following requirements **Error! Reference source not found.**:

- large number of channels has to be equipped; channel Count per detector unit: 500 (200 mm wide detector), 950 (380 mm wide detector); for all detector units approx. 47k channels.
- Has to be close to the detector to avoid signal transmission over large distances.
- Individual detector systems are distributed over several meters connections should be fully optical.
- Read-Out Framework is MBS (standard Data Acquisition System at GSI [11])
- The Application count-rate is several MHz.
- The Timing Reference is in the long term White Rabbit **Error! Reference source not found.**.
- In-vacuum operation is required.
- Radiation hardness is preferable.

Furthermore, simulations have been performed to determine the needed dynamic range of the charge measurement (see chapter 10). The spatial resolution in x coordinate is directly given by the design of the GEM TPC, Pad Plane (pitch of 0.4 mm). Since the standard deviation (σ) of a `uniform distribution' is w/√12 (with w the width) one obtains: σx=0.12 mm or FWHM x=2.355×σx =0.27 mm. The y coordinate is determined from the time measurement (y = vdrift × tdrift) to obtain a similar spacial resolution as for x a time resolution below 3 ns is needed (see Table 2.2). This upper limit includes contribution from the electronics and the detector, since the electronics should not be the dominating factor the resolution should be below 1 ns (σt;elec < 1 ns).

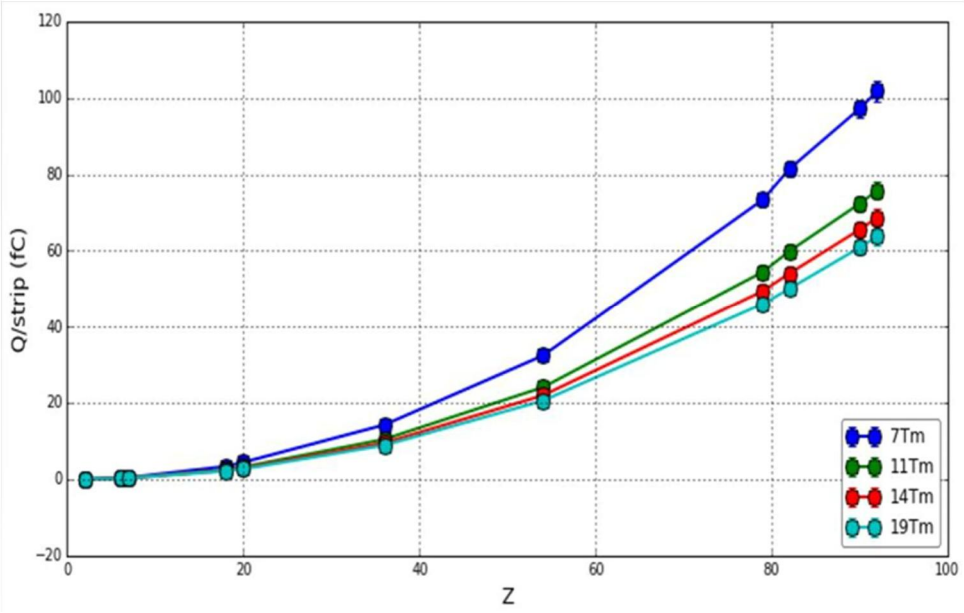

Figure 9.1: shown is the charge per strip, which gives the needed dynamic range of the electronics. 16% from total (center strip receives 13% - 17% depending on drift length and specs).

9.1. Developments of pre-series

So far an N-XYTER [13] based electronic board called GEMEX [10][14] was used for tests of the first SuperFRS GEM TPC. The N-XYTER chip has been selected as ASIC since it offers 128 independent readout channels on a very compact chip (the die size is 6.5 mm × 3.1 mm). Furthermore, there is in-house experience with this ASCI, giving us the unique opportunity to design the full board together with the ASIC developers.

The GEMEX comprises two N-XYTER chips an ADC and a FPGA read-out chain based on the EXPLODER [15] card. It is a 256 channel front end board which hosts trigger and timestamp logic and an external clock input to a FPGA and a high precision PLL (Phase Locked Loop) synthesizer. As in the N-XYTER chip the digitization is performed with a sampling rate of 32 MHz with 12 bit resolution and dynamic range up to 1.2 × 105 electrons.

The readout of the buffered data is synchronized to a 32 MHz clock in a token ring. The token ReadOut Controller (ROC) registers if there are data in the buffers of one NXYTER channel. In each clock cycle, the data of one channel is sent via a data bus to the FPGA. In that way, a readout rate of 250 kHz per channel is reached (32 MHz / 128 = 250 kHz) [16].

Each of the boards comprises a 300 pin connector, where up to 256 detector signals can be connected, the remaining free pins are e.g. used to supply the electronics with low voltage.

Due to the temperature drift of the baseline of the chip cooling needs to be provided. The heat management of the GEMEX card is realized by a partial solid backing of copper and direct mounting of the ASICs on the heat spreader. Due to stringent spatial restrictions heat produced is taken away effectively via the edges where an active fluid cooling system is flanged to the surfaces [10],[13].

The main issue with the applied electronics is the dynamic range. Here, as mentioned, it is 1.2 × 105 - which expressed in charge units leads to range of about 25 fC, see Fig. 9.1.

The more general requirements given in the previous section become more specific for the above mentioned readout design:

- FEB amount required (a 256 ch) in total: 185
- Reference Clock for FPGA and ASIC is required.
- ASIC: N-XYTER 2.0
- (Fluid) cooling is needed.
- Protection of ASIC: minimum glob-topped, packaged possible.
- Powering-scheme & -sequence: first N-XYTER then FPGA.
- Software feature: N-XYTER emulation and ADC emulation.
- Internal AND External pulser: Required for probing the N-XYTER/ADC range.

• N-XYTER Monitoring Channel: N-XYTER exhibits a channel with full accessibility to the analog part of signal processing path.

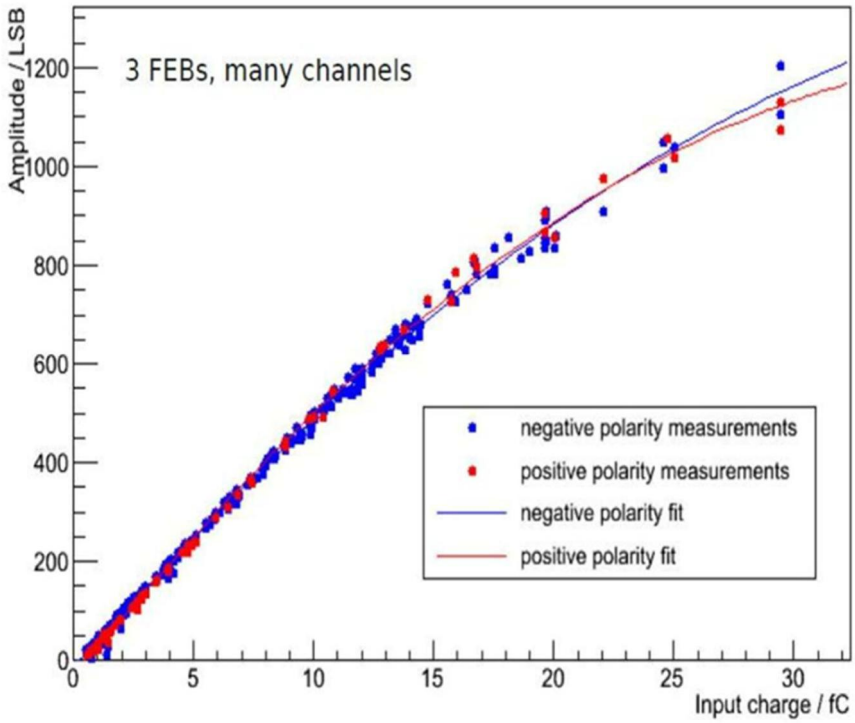

Figure 9.2: shown is the calibration of the N-XYTER 2.0 [17][18].

9.2. Outlook on the development of the readout electronics

The last version of the readout electronics (GEMEX 1c) showed several problems and was unfortunately never fully functional. The production of the board is due to the following facts very challenging:

- Very compact design (PCB form-factor).
- Stacking of materials: `partial solid backing of copper' (for cooling).
- ASIC mounting/bonding `pitch adapter' needed (N-XYTER has a 50 m inter-channel pitch).
- The used `Samtec BSH (edge mount) 300pin connector' cannot be soldered by machines.

The integration of N-XYTER, FPGA and the compact design plus a difficult to mount connector increased the probability that one of the components caused the full board to not function correctly. Furthermore, the following two difficulties let to the fact that the few produced samples worked in an erroneous state:

- The cooling requirements were very high.
- The powering sequence (N-XYTER first, then FPGA) and scheme (on board) was not working.

All the above mentioned points made a revision of the board mandatory. Furthermore, in the next version of the readout electronics two components will be replaced:

- Instead of the former used FPGA a XILINX Spartan 6 (same as used for Exploder) will be used. This FPGA is larger and it makes the transformation of the `Exploder software' more convenient.
- The N-XYTER 1.1 will be exchanged by the N-XYTER 2.0, which is much more stable with temperature.

These aspects lead to a scheme in which we separate the above mentioned problems on three single boards, respectively, see Fig. 9.3 and also go back to a space-wise more relaxed design.

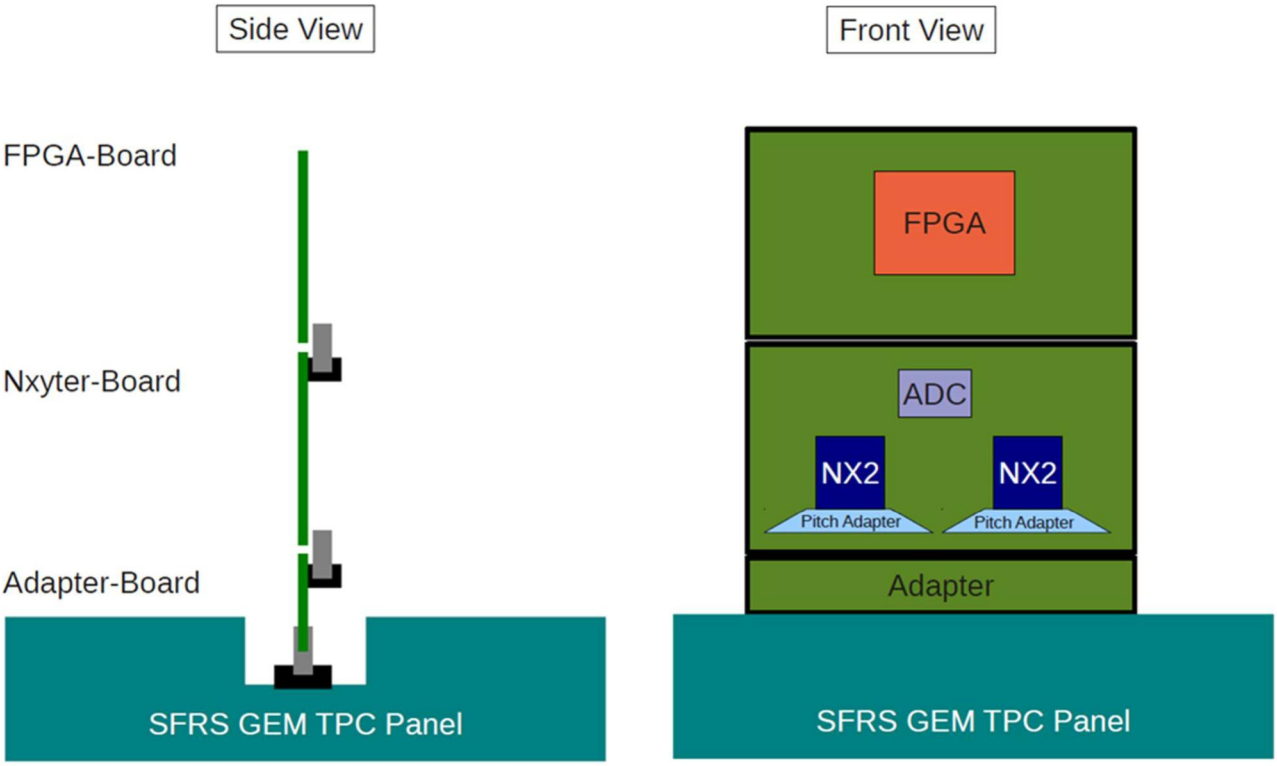

Figure 9.3: Design scheme for the next version of the readout electronics.

The new design offers the following advantages:

- components can be tested individually:
- Standalone test of new FPGA.
- Standalone test of (new) N-XYTER 2.0.
- The connector in between gives access to all signals (e.g. between N-XYTER and FPGA).
- More space available on PCB:
- makes cooling easier

- makes usage of larger FPGA possible
- gives space for more test pads
- Production of individual PCBs is easier. Separation of the difficult production processes to different boards minimizes risk for production failure
- separation of boards makes division of work easier (ASIC experts / FPGA experts)

The issue with the too small dynamic range will be solved with a controllable add-on `pre-attenuator card.

10. Simulation and detector performance

10.1. TPC current performance

The currently used tracking detector at the FRS is TPC type detector with delay lines readout. The x-coordinate is determined from the time of signal arrival from the delay lines, y-coordinate is calculated from the drift time through the drift volume. The drift volume is filled usually by P10 gas mixture. The delaylines are used for unambiguous determination of the position and noise or false signal rejection. The signals are read and digitalized by conventional electronics. The details on the construction and detector read-out can be found in [1].

The TPC detector can be used for tracking the projectiles from proton to U. The measured position reconstruction efficiency as a function of ^{238}U ions rate at 1 GeV/u is shown in Fig. 10.1. The tracking efficiency of more than 99% was achieved up to 40kHz and efficiency of 90% up to 250kHz.

The spatial resolution of the TPC detector was estimated from the correlation of the multiple measurements (see [1] for details). The achieved spatial resolution in x-coordinate was 88m and 38m in y-coordinate for Ar and Kr projectiles. The distributions of the multiple measurements differences are shown in Fig. 10.2.

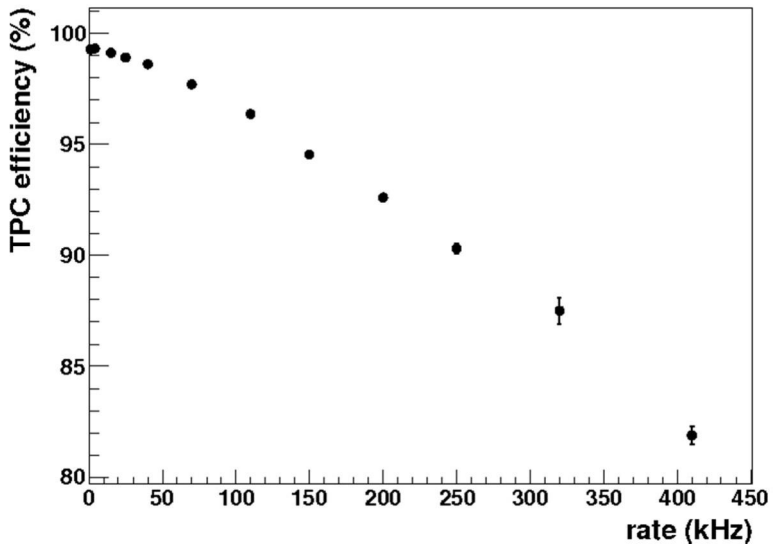

Figure 10.1: Tracking efficiency as a function of 238U ions rate at 1 GeV/u. As a reference plastic scintillator was used.

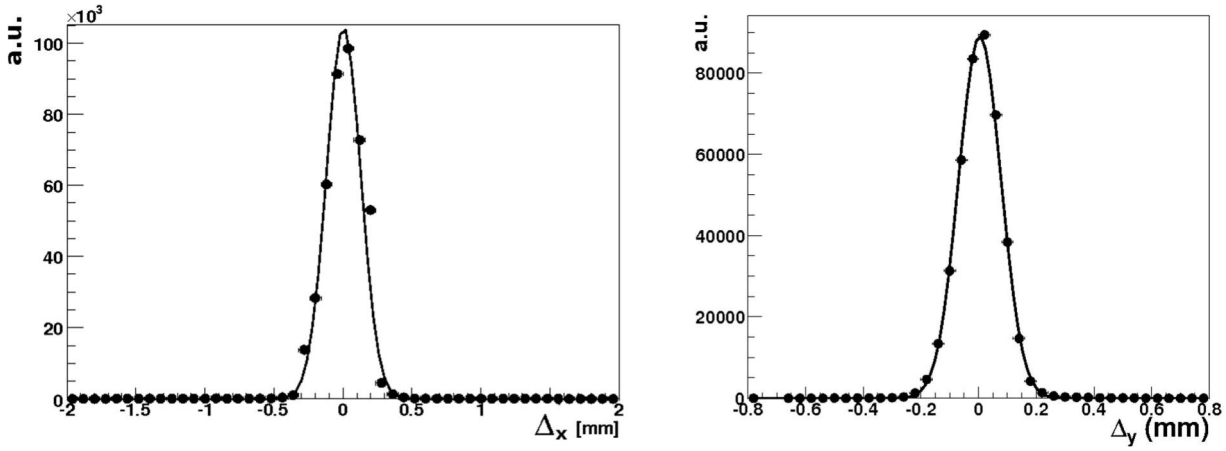

Figure 10.2: Top: Position resolution in x-direction for Ar ions rate at 1 GeV/u $\sigma_x = \frac{\sigma_{\Delta x}}{\sqrt{2}} = 0,088\ mm$. Bottom: Position resolution in x-direction for K r ions rate at 1 GeV/u $\sigma_y = \frac{\sigma_{\Delta y}}{\sqrt{2}} = 0,038\ mm$.

10.2. Simulation of requirements for Super-FRS tracking

10.2.1. Geometry and parameters

The whole design of the detector is highly modular and as compact as possible in order to minimize the overall space requirements in view of the later conditions to be faced at the Super-FRS. During installation only very little manual interactions are required to potentially exchange faulty parts. Except for the flaps of the framed GEM-foils in the GEM-stack no electrical connection has to be done explicitly and only one fluid connector (gas out) needs to be joined.

The following parameters were used in the simulations:

Active volume: 400 mm x 80 mm x 30 mm

Active volume gas: P10 at normal temperature and pressure

P10 mean ionization potential W_i = 26.2 eV

P10 density ρ = 1.7 mg/cm^{-2}

10.2.2. Charge deposition

The charge deposition in an active volume of the Super-FRS tracking detector was calculated from the projectile energy loss (dE). The projectile energy loss was obtained from ATIMA [19]. The dE does not fully correspond to the deposited energy in the active volume of the detector. The projectile energy loss needs to be corrected for the energy taken away, ie by delta electrons. The correction depends on the projectile type, energy, geometry of the active volume and was calculated using GEANT4[20]. The amount of deposited energy and width calculated for several projectiles at different energies are shown in Fig. 10.3.

The number of produced electrons from ionization (Q_i) of projectiles are calculated from deposited energy and mean ionization potential:

$$Q_i = \frac{E_D}{W_i} \qquad (1)$$

Where W_i is mean ionization potential.

The calculated charge deposited inside the active volume for different projectiles and magnetic rigidities (energies) is shown in Fig. 10.4.

The deposited charge in the active volume will be spatially scattered until it reach the induction gap and the pad plane. The main contributions to the spread are coming from diffusion in the drift space and spatial straggling in the GEM stack. The field in the drift space can be regarded as constant, with electric field of 400V/cm. The deviations from non-uniform field are negligible according to the FEM calculation. The spatial spread in the GEM stack was calculated using FEM method (electric field calculation) and Garfield (electron transport). The total spatial spread can be approximated by:

$$\sigma_{ex} = \sqrt{0.359 \cdot Y + 0.1225} \qquad (2)$$

Where ρ_{ex} is spatial spread of the electrons at the induction gap in mm, Y is the drift length in cm.

The deposited charge after the drift and GEM stack will induce current and charge on the pad plane. The assumed parameters of the pad plane are: width of the strip = 0.25mm, pitch p = 0.4mm and strip length along beam axis = 30mm). The induction gap is 2mm with electric field of 3kVcm. The center of the beam is assumed to be over the centered beam, which received the most of the charge. The calculation was done using GARFIELD. The relative induced charge on the strips as a function of strip number is shown Fig. 10.5. The maximum charge will be collected by central strip and the total amount range from 13-17% depending on the drift length. This numbers are used to calculate induced charge per strip from the total deposited charge calculated using Eq. 1. The induced charge on the central strip assuming 16.6% collection from the total deposited charge for different projectiles at different magnetic rigidities are shown in Fig. 10.6. The simulation suggest the readout needs to handle 100fC signal from the strip assuming P10 gas mixture and minimum working rigidity around 7Tm.

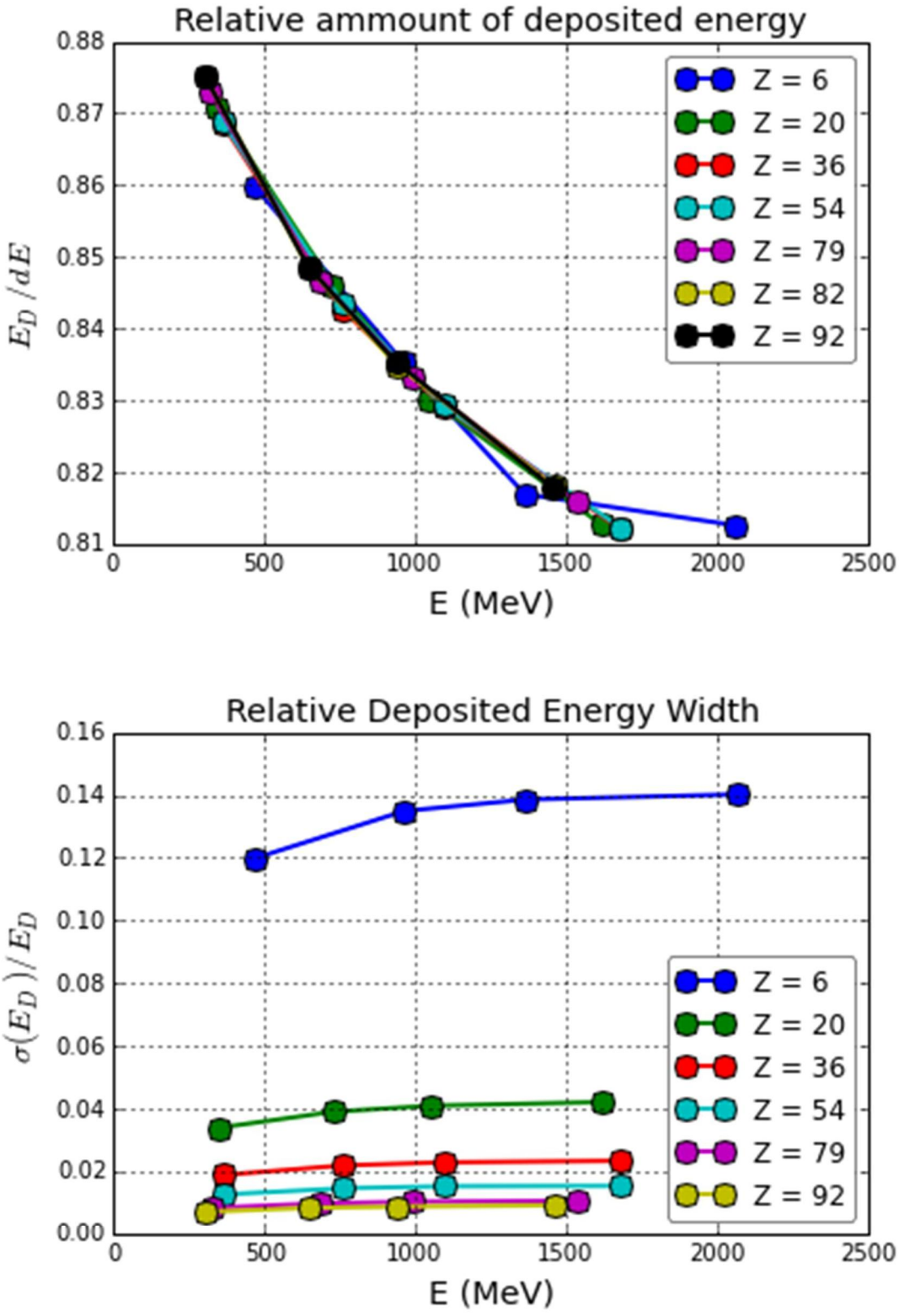

Figure 10.3: Top: The calculated relative deposited energy as a function of energy and charge of the projectile. Bottom: The calculated width of the deposited energy as a function of energy and charge of the projectile.

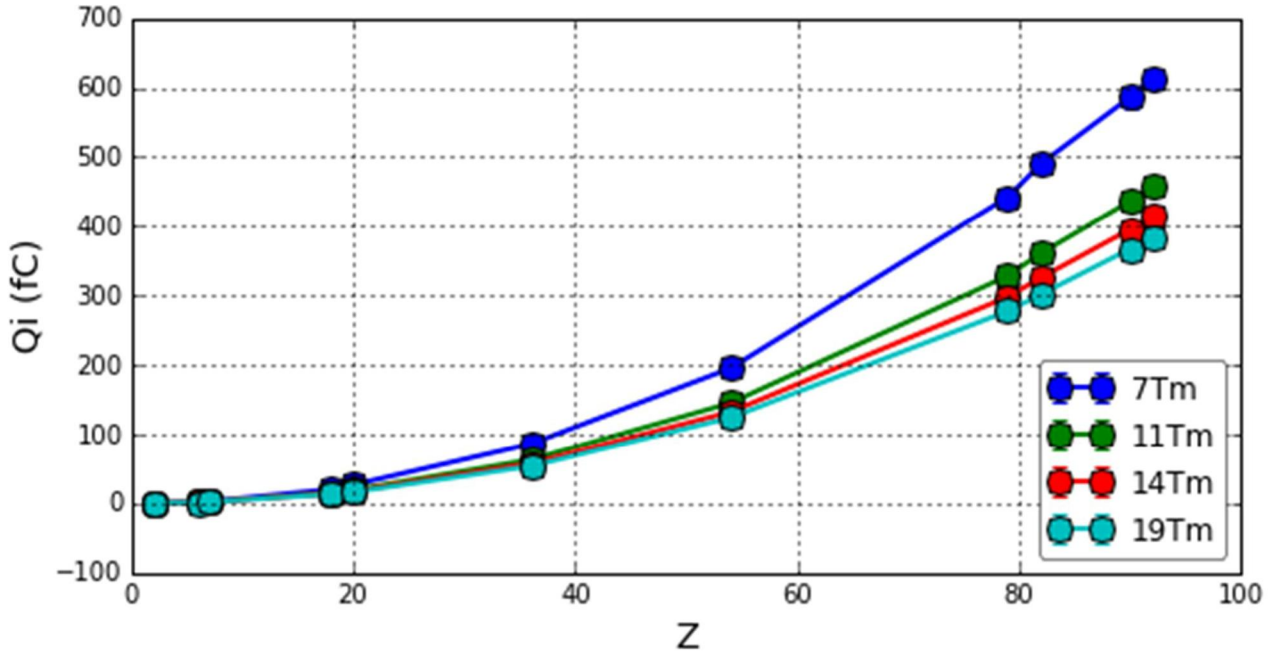

Figure 10.4: The total charge deposited in the active volume of the detector for different ion and energies.

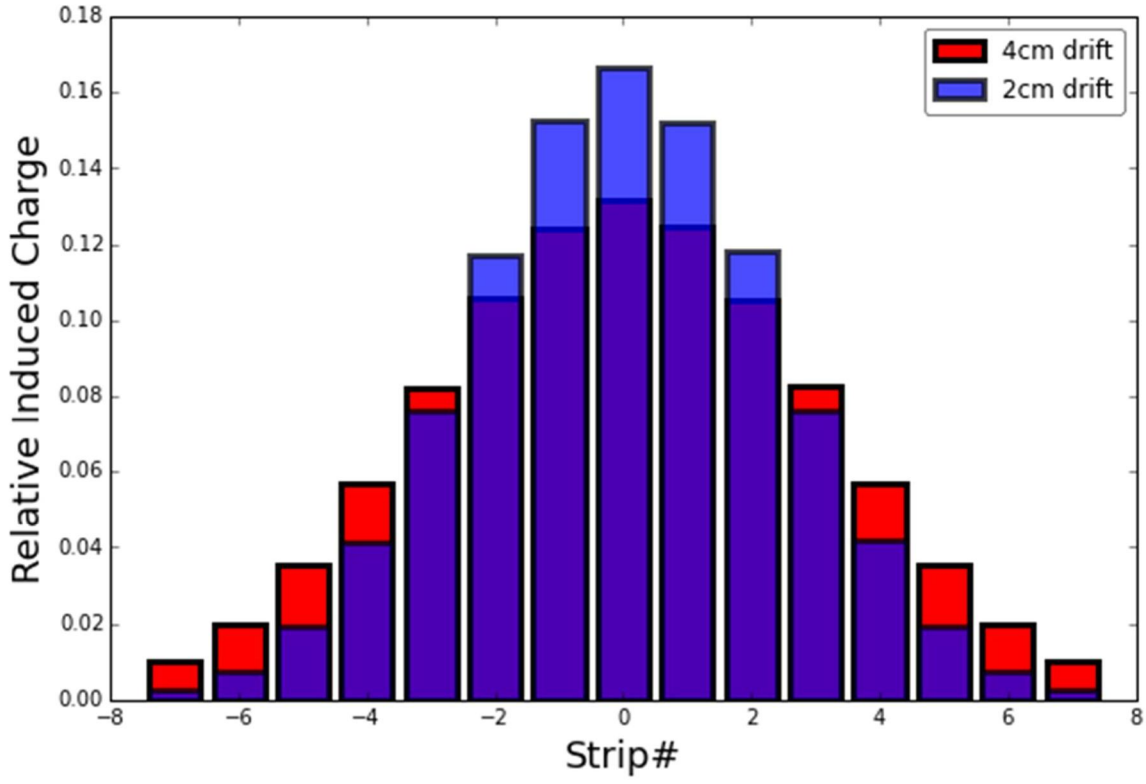

Figure 10.5: The relative induced charge on the padplane strips. The red corresponds to the 4cm drift, blue to 2cm drift.

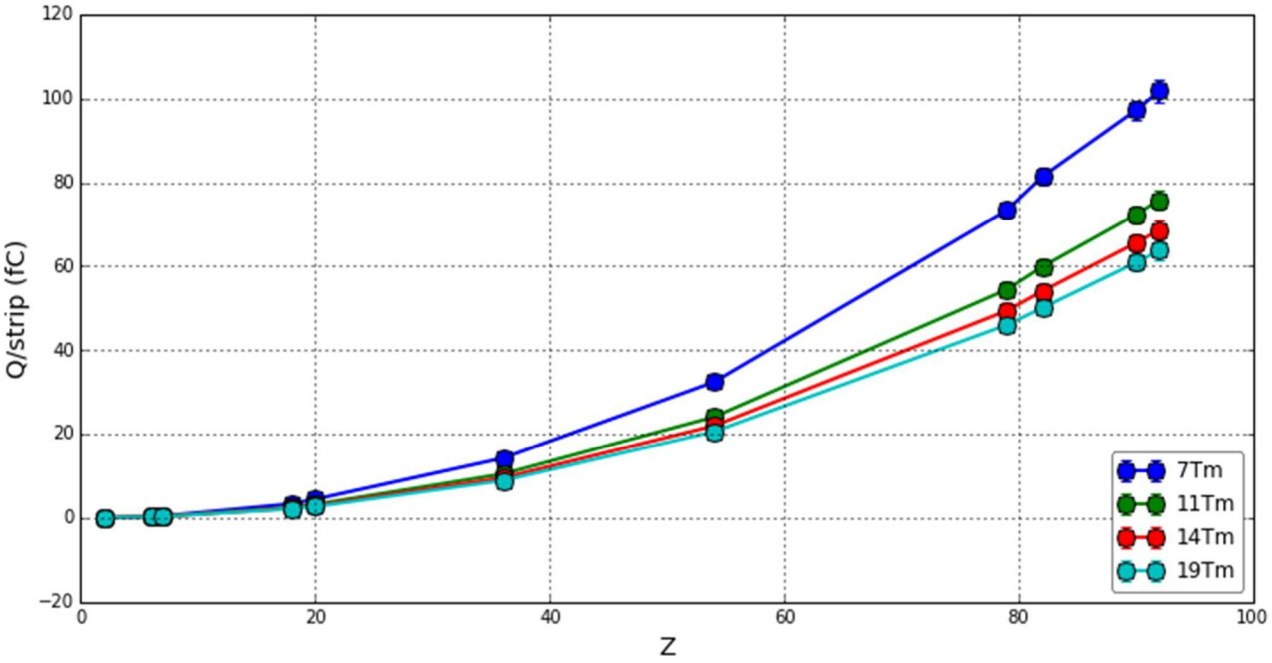

Figure 10.6: The induced charge per strip assuming the 16.6% charge collected from the total amount.

10.2.3. Angular resolution

For the angular reconstruction of the projectile two tracking detectors are used at the focal planes of the Super-FRS. The angular resolution of the two TPC detector function of distance between the detectors and their position resolution is plotted in the Figure 10.7. The calculation assumes no additional matter between the tracking detectors. The minimal distance between the tracking detectors according to current Super-FRS design is 1.3m. In that case the position resolution of 0.2 mm corresponds to the angular reconstruction at focal plane around 0.2 mrad.

10.2.4. Angular resolution

The assumed detector materials are: 2x100μm Fe window, 5x20μm mylar foil, 40cm of P10 gas. The position and angular straggling were calculated using ATIMA. The position straggling in the middle of the detector caused by angular straggling in half of the matter is show in Figs 10.8 (left). This corresponds to the additional uncertainty of the measured position to the intrinsic position resolution. The angular straggling due to whole detector matter is shown in Fig 10.8 (right).

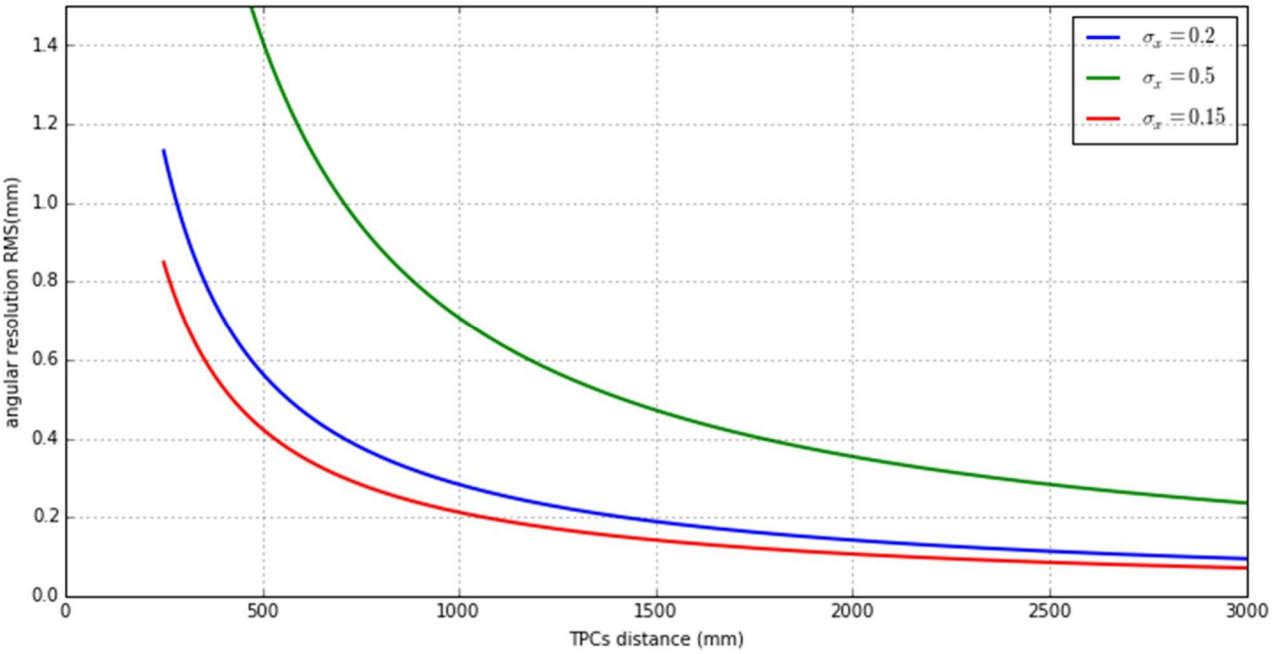

Figure 10.7: The angular resolution of the tracking detectors as a function of detector distance and position resolution.

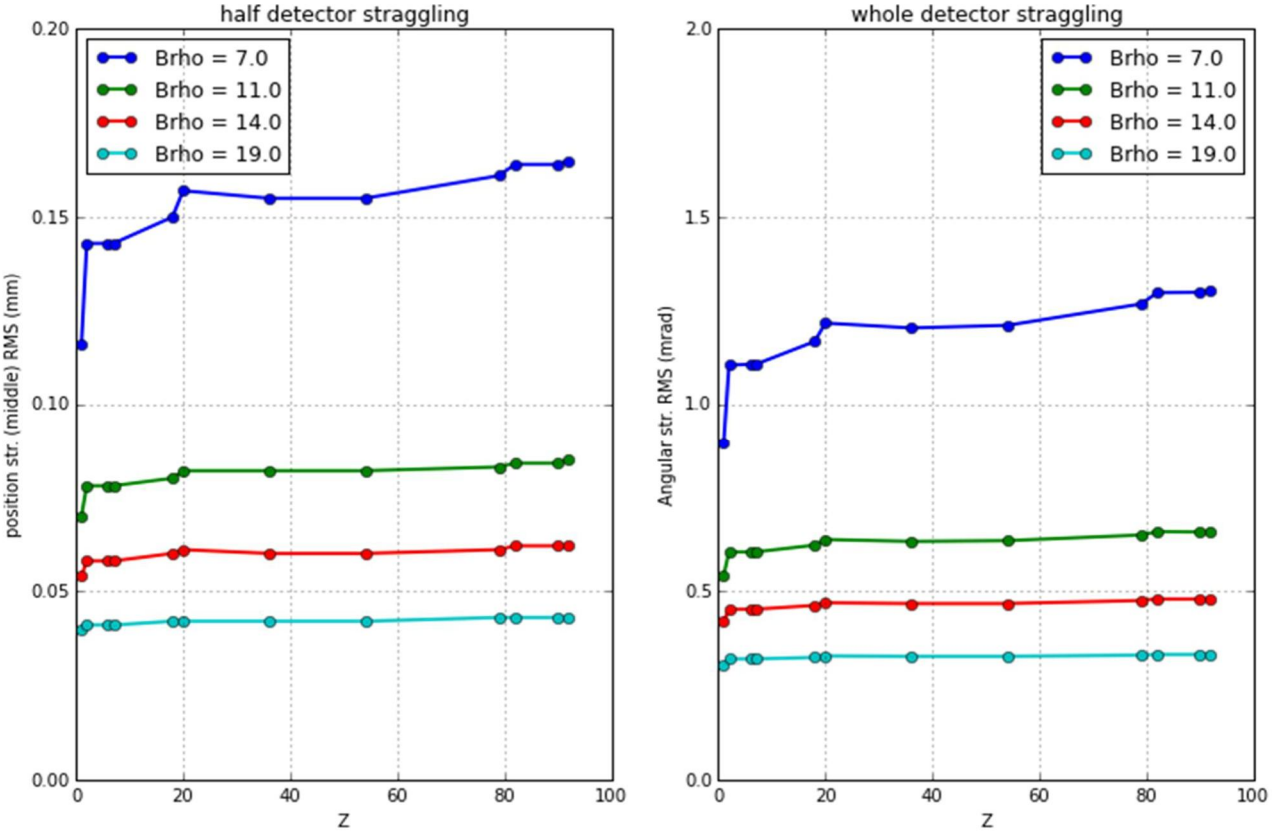

Figure 10.8: Left: The position straggling at half of the detector. Right: Angular straggling after passing the whole detector.

10.3. Twin design and control sum

To improve the efficiency at high rates of the standard TPC [21] and possibly future tracking detector so called Twin design is proposed [22]. This allows calculating a Control Sum which is in principle sum of the drift times from the drift volumes. As the sum should be a constant it can be used for pile-up and noise rejection and for multi-hit track reconstruction. The Control Sum was calculated as $t_{CS} = t_1 + t_2 - 2\,t_t$, where t_1 and t_2 are drift times from the two drift spaces and t_t is the reference time coming from scintillator. All times are measured in multi-hit mode. The Twin design and multi-hit electronics allows recovering the tracking efficiency at high rates up to MHz level. The TwinTPC prototype read by delay lines and conventional electronics were built at Comenius University Bratislava and already tested at the FRS. The test was done using Au beam at 700MeVu. The particle rate was estimated from the number of hits registered by the plastic scintillator. The drift time resolution derived from the control sum width as a function of particle rate is shown in Fig. 10.9. The worse resolution at higher rate can be caused by distortion due to space-charge at higher rates.

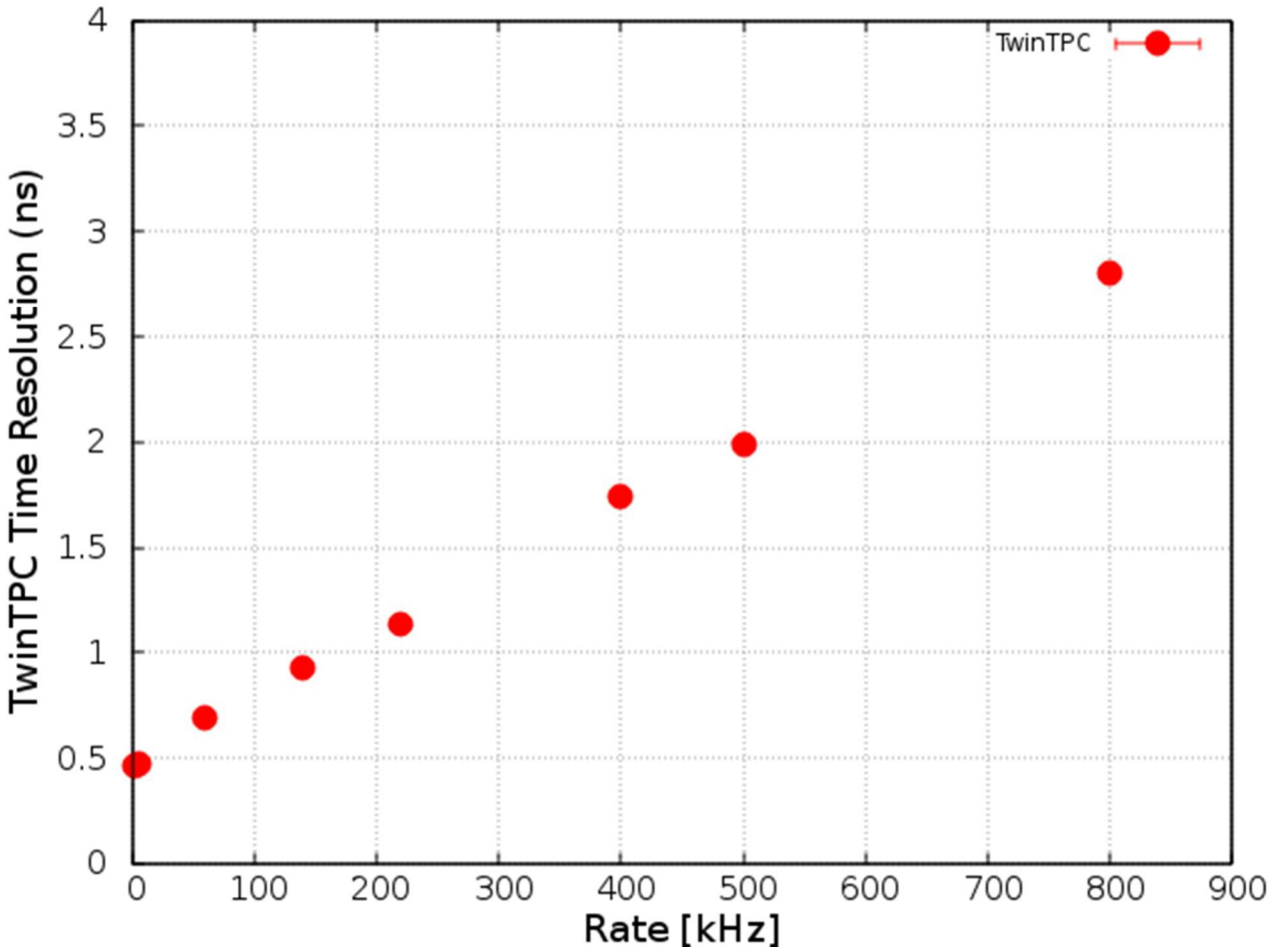

Figure 10.9: Time resolution of the drift time measurement as a function of rate. The time resolution was estimated from the from the anode difference between the opposite drift volumes.

In addition to that the Control Sum measured with the Twin GEM-TPC (HGB4) during the campaign S417 at GSI is shown in Fig. 10.10. The primary particles were Uranium and moderate rate.

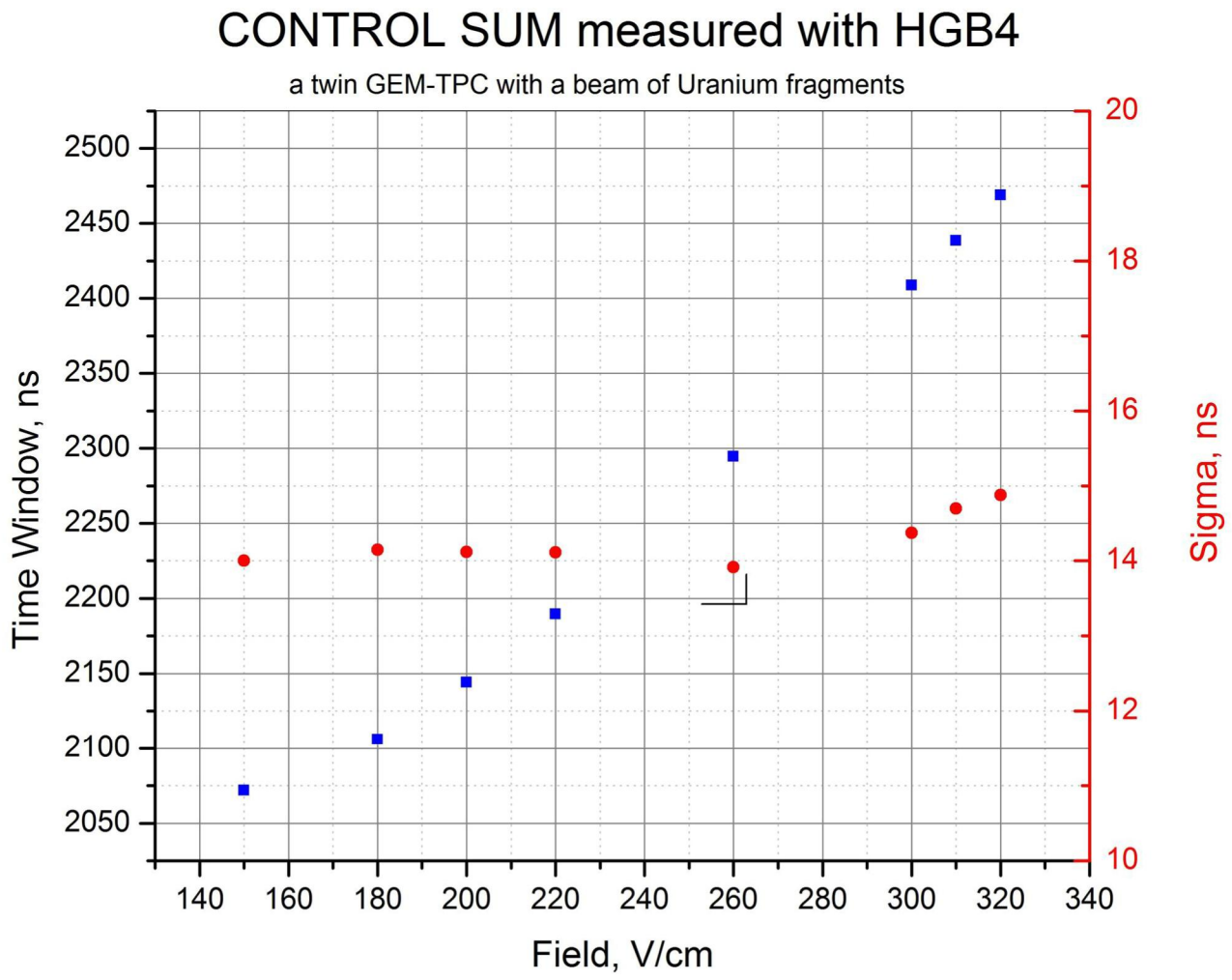

Figure 10.10: The control Sum scan at different fields; from 150 V/cm up to 320 V/cm. In blue the total sum and on red the time resolution.

Appendix I

The Super-FRS is the central device of the NUSTAR facility at FAIR **Error! Reference source not found.**. It will be used to produce rare isotope beams from projectile fragmentation and from in-flight fission of uranium with energies up to 1.5 GeV/u. It is expected to deliver exotic nuclei to three branches: the Low-Energy Branch (LEB), the High-Energy Branch (HEB) and the Storage-Ring Branch (RB). The three branches are shown in Fig. 11.1.

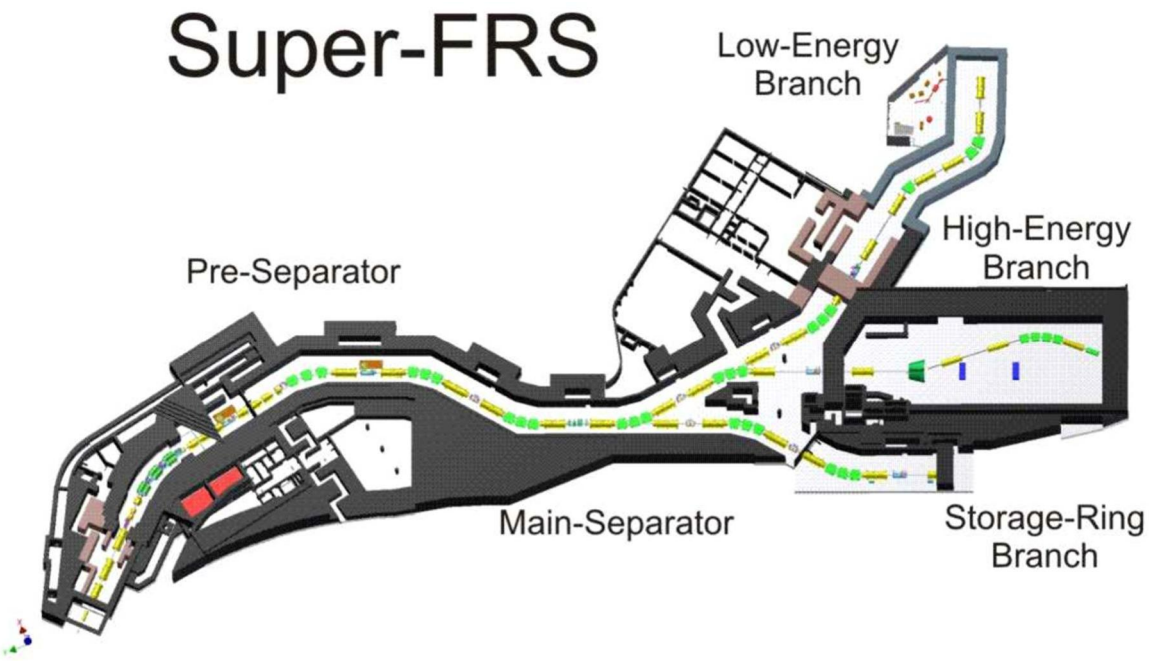

Figure 11.1: Layout of the Super-FRS.

To produce in-flight rare isotope beams (RIBs), the primary beam delivered by the SIS100 (e.g. $3x10^{11}$ $^{238}U/s$) will impinge on a graphite target of a few g/cm^2 located at the entrance of the Super-FRS. The high-separation power of the device will allow to deliver high-quality RIBs spatially separated within a few hundreds nanoseconds. For these dedicated experimental branches, the Super-FRS will provide spatially separated mono-isotopic or cocktail beams RIBs depending on the goals of the experiments. Challenging requirements from experiments at those branches are achieved with a multi-stage magnetic system, comprising intermediate degrader stations.

The main parameters of the Super-FRS are listed in Table 11.1.

Magnetic rigidity range	2-20 Tm
Horizontal emittance	40π mm mrad
Vertical emittance	40π mm mrad
Momentum acceptance	+/- 2.5 %
Horizontal angular acceptance	+/- 40 mrad
Vertical acceptance	+/- 20 mrad
First order resolution first stage (for 2 mm^2 target)	750
First order resolution second stage (for 2 mm^2 target)	1500
Momentum dispersion (FMF2-FHF1)	7.6 cm /%
Horizontal magnification (FMF2-FHF1)	1.45
Length of Pre-Separator	≈71 m
Length of the Main-Separator (HEB)	≈105 m

Table 11.1: Main parameters of the Super-FRS.

Specialized detector systems for full particle identification will verify the separation performance. The fragments are uniquely identified in charge Z and in mass numbers A by using the so-called Bρ-ΔE-ToF method. According to this method one can distinguish three classes of detectors. Particle identification at the Super-FRS will be achieved by using precise Tracking Detectors to measure positions and angles at focus, Multi-Sampling Ionization Chamber (MUSIC) for ΔE measurements and Time-of-Flight (ToF) detectors to measure the fragment velocity. Their combined information allows ion identification on event by-event basis as well as the measurement of the ion momentum. Details about the particle identification are given in [23]. The physics goals of the NUSTAR collaboration are given in Appendix II [24][25].

Appendix II

NUSTAR physic cases

- **Super-FRS collaboration**: The selected experiments can be pursued exclusively at FAIR with Super-FRS, due to the combination of high energies, high momentum-resolution and the characteristics of the multiple-stage magnetic spectrometer. Examples are the study of exotic atoms (mesonic nuclei), exotic hypernuclei, high-momentum components of the tensor force, delta resonances in asymmetric nuclear matter, resonant coherent excitation in crystals, and in-flight decays in extremely short-lived nuclei and resonance states. Important are production of new isotopes and atomic collision studies (stopping, straggling) with heavy fragment beams at the highest energies of FAIR.

- **HISPEC/DESPEC** (**Hi**gh-Resolution **Spec**troscopy**/De**cay **Spec**troscopy): The aim is to comprehensively benchmark nuclear models and the r-process along and beyond N=126, and along neutron-rich Z~82 isotopes.

- **MATS/LaSpec** (Precision **M**easurements of very short-lived nuclei with **A**dvanced **T**rapping **S**ystem**)/Las**er **Spec**troscopy): It is expected that LaSpec and MATS will be competitive especially in the regions of neutron-rich refractory elements, which cannot be delivered from ISOL-type facilities in large amounts. This is an interesting region to study because for example, around ^{108}Zr, new shape evolutions (from very deformed nuclei to spherical ones) are theoretically predicted. The region east and northeast of lead - especially beyond N=126 - is of high interest concerning the r-process path.

- **R^{3}B** (**R**eactions with **R**elativistic **R**adioactive **B**eams): Specific examples of the R^{3}B physics program are quasi-free scattering reactions, dipole response and dipole polarizability of heavy neutron-rich nuclei, the study of the dipole response of ´halo´ nuclei up to high excitation energies of 30 MeV, electromagnetically-induced fission, and the measurement of the fission barriers.

- **ILIMA** (**I**someric beams, **LI**fetimes and **MA**sses): ILIMA will be unique worldwide for the study of short-lived nuclei enabling masses and half-lives to be measured for the first time. In particular, this is true for nuclei with A~200 that are key to understanding the heaviest (A~195) r-process abundance peak.

- **EXL/ELISe** (**Ex**otic nuclei studied in **l**ight-ion induced reactions at the NESR storage ring/ **El**ectron-**I**on **S**catt**e**ring in a Storage Ring): low momentum transfer measurements with recoil particles with energies below 500 keV can be performed in a storage ring to investigate properties such as the nuclear compressibility of medium-heavy and heavy isotopes.

Appendix III

The GEMTPC prototype in-beam test

The prototypes were tested with the 197Au beam at 750 MeV/u at the middle focal plane of the FRS. The prototypes were tested in air at normal pressure. The standard TPCs were used as a reference tracking detectors. As a working gas the P10 mixture was used for all detectors. The setup of the test is shown in Fig. 12.1. Additionally the plastic scintillator was installed before the setup for the triggering and timing purposes.

The reference trackers were used to deduce the position resolution of the prototypes. The data were taken for several settings of the prototype and are summarized as a function of position at the detector in Fig. 12.2. The obtained position resolution for the prototype over the whole active volume was below 0.2mm (RMS)

The plastic scintillator was used to determine the efficiency. The data were taken at moderate rate of 60kHz. For this rate the efficiency more than 99% was obtained for both detectors and whole active volume. The obtained efficiencies as a function of position at the detector for several runs are summarized in Fig. 12.3.

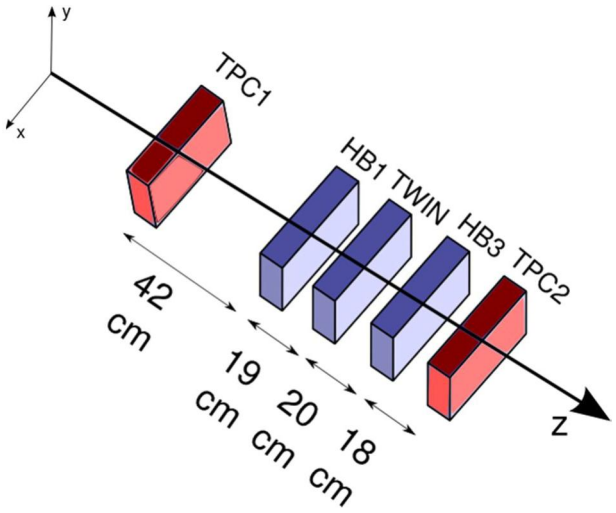

Figure 12.1: The setup of in-beam test of the GEMTPC prototype.

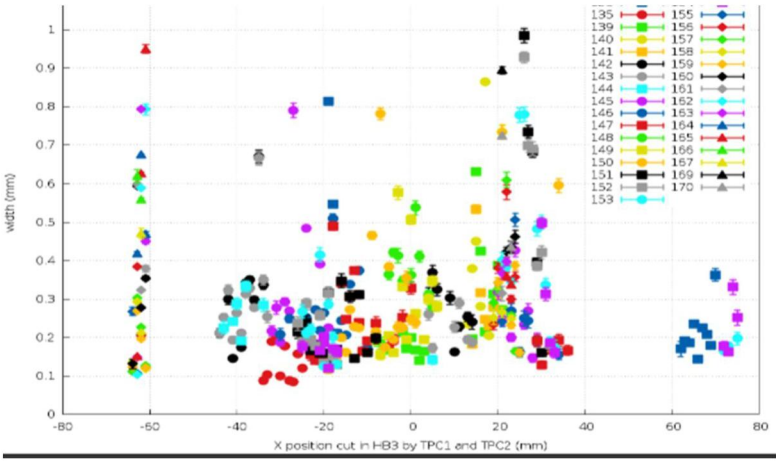

Figure12.2: The measured position resolution of the GEMTPC prototype for different runs and position at the detector

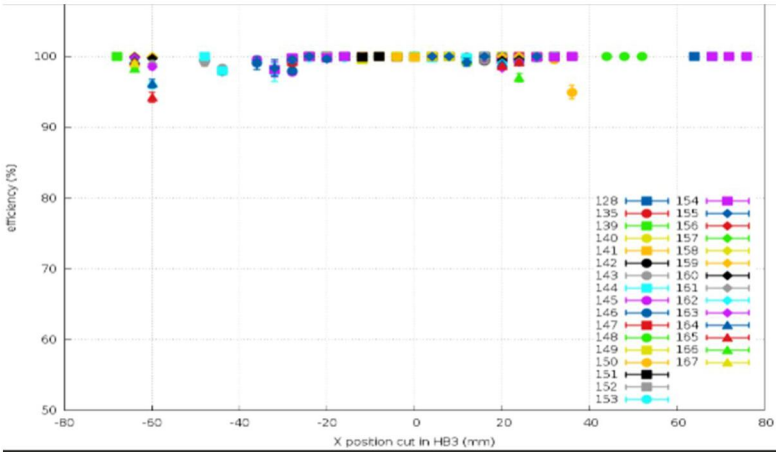

Figure 12.3: The measured efficiency of the GEMTPC prototype for different runs and position at the detector

References

[1] http://www.fair-center.de/index.php?id=186&L=0

[2] F. Garcia et al. “GEM-TPC Prototype for Beam Diagnostics of Super-FRS in NUSTAR Experi-ment - FAIR”. In: Nuclear Science Symposium Conference Record (NSS/MIC), 2009, IEEE. 2009, pp. 269–272. DOI: 10.1109/NSSMIC.2009.5401762.

[3] F. Garcia et al. “Prototype development of a GEM-TPC for the Super-FRS of the FAIR facility”. In: Nuclear Science Symposium Conference Record (NSS/MIC), 2011, IEEE. 2011, pp. 1788–1792. DOI: 10.1109/NSSMIC.2011.6154683

[4] http://www.fair-center.eu/en/public/experiment-program/nustar-physics/superfrs.html

[5] M. G. Bagliesi et al. “The TOTEM T2 telescope based on triple-GEM chambers”. In: Nucl. Instr. Meth. A 617.1-3 (2010), pp. 134–137. DOI: 10.1016/j.nima.2009.07.006.

[6] http://cds.cern.ch/record/1622286/files/ALICE-TDR-016.pdf

[7] C. Altunbas et al. “Construction, test and commissioning of the triple-GEM tracking detectors for COMPASS”. In: Nucl. Instr. Meth. A 490.1-2 (2002), pp. 177–203. DOI: 10.1016/S0168-9002(02)00910-5.

[8] M. Alfonsi et al. “The triple-GEM detector for the M1R1 muon station at LHCB”. In: Nuclear Science Symposium Conference Record (NSS/MIC), 2005, IEEE. 2005, pp. 811–815. DOI: 10.1109/NSSMIC.2005.1596379.

[9] Z. Fraenkel et al. “A hadron blind detector for the PHENIX experiment at RHIC”. In: Nucl. Instr. Meth. A 546.3 (2005), pp. 466–480. DOI: 10.1016/j.nima.2005.02.039.

[10] Voss, B., Baraki, F., Ernst, B., Garcia, F., Hoffmann, J., Kleipa, V., Kunkel, J., Kurz, N., Ndiaye, S., Prochazka, A., Rusanov, I., Schmidt, C.J. Shizu, M., Skott, P., Soyk, D., Tchatcho, C. GSI Scientific Report , 247 (2011).

[11] Kurz, N. https://www.gsi.de/mbs/.

[12] Serrano, J., Alvarez, P., Cattin, M., Garcia Cota, E., Lewis, J., Moreira, P., Wlostowski, T., Gaderer, G., Loschmidt, P., Dedic, J., Bär, R., Fleck, T., Kreider, M., Prados, C., and Rauch, S. In International Conference on Accelerator and Large Experimental Physics Control Systems (ICALEPCS), (2009).

[13] Brogna, A. S., Buzzetti, S., Dabrowski, W., Fiutowski, T., Gebauer, B., Klein, M., Schmidt, C. J., Soltveit, H. K., Szczygiel, R., and Trunk, U. Nuclear Instruments and Methods in Physics Research A 568, 301-308 November (2006)

[14] Hoffmann, J. https://www.gsi.de/fileadmin/EE/Module/EXPLODER/exploder3_v4.pdf

[15] Hoffmann, J. https://www.gsi.de/fileadmin/EE/Module/GEMEX/gemex1.pdf

[16] Schrock, P.; The Electric Dipole Response of ^{132}Sn, PhD thesis, Technische Universität Darmstadt, Germany, (2015).

[17] Dementyev, D., Krylov, V., Löchner, S., Schmidt, C. J., and Sorokin, I. GSI Scientific Report , 286 (2012).

[18] Dementyev, D. http://icssnp.mephi.ru/content/le/2014/section11/11 09 Dementyev.pdf, (2014).

[19] https://web-docs.gsi.de/weick/atima/

[20] http://geant4.cern.ch/

[21] R.Janik et al., Nucl. Instr. and Meth. A640(2011)54-57

[22] Prochazka et al., GSI Report 2013-1, 174 p. (2013)

[23] C. Nociforo, 2014 JINST 9 C01022.

[24] N. Kalentar-Nayestanaki, on behalf of the NUSTAR collaboration, Opportunities for NUSTAR@FAIR - December 2014.

[25] Super-FRS collaboration, Scientific program of the Super-FRS collaboration: report of the collaboration to the FAIR management – September 2014.